

Laboratory Experiments to Evaluate Diffusion of ^{14}C into Nevada Test Site Carbonate Aquifer Matrix

Prepared by

Ronald L. Hershey, William Howcroft and Paul W. Reimus

submitted to

Nevada Site Office
National Nuclear Security Administration
U.S. Department of Energy
Las Vegas, Nevada

MARCH 2003

Publication No. 45180

Reference herein to any specific commercial product, process, or service by trade name, trademark, manufacturer, or otherwise, does not necessarily constitute or imply its endorsement, recommendation, or favoring by the United States Government or any agency thereof or its contractors or subcontractors. The views and opinions of authors expressed herein do not necessarily state or reflect those of the United States Government or any agency thereof.

This report has been reproduced directly from the best available copy.

Available for sale to the public, in paper, from:

U.S. Department of Commerce

National Technical Information Service

5285 Port Royal Rd.

Springfield, VA 22161

phone: 800.553.6847

fax: 703.605.6000

email: order@ntis.fedworld.gov

online ordering: <http://www.ntis.gov/ordering.htm>

Available electronically at <http://www.doe.gov/bridge>

Available for a processing fee to the U.S. Department of Energy and its contractors, in paper, from:

U.S. Department of Energy

Office of Scientific and Technical Information

P.O. Box 62

Oak Ridge, TN 37831-0062

phone: 423.576.8401

fax: 423.576.5728

email: reports@adonis.osti.gov

Laboratory Experiments to Evaluate Diffusion of ^{14}C into Nevada Test Site Carbonate Aquifer Matrix

Prepared by

Ronald L. Hershey and William Howcroft
Division of Hydrologic Sciences
Desert Research Institute
University and Community College System of Nevada

and

Paul W. Reimus
Chemical Sciences and Technology Division
Earth and Environmental Sciences Division
Los Alamos National Laboratory

Publication No. 45180

Submitted to

Nevada Site Office
National Nuclear Security Administration
U.S. Department of Energy
Las Vegas, Nevada

March 2003

The work upon which this report is based was supported by the U.S. Department of Energy under Contracts #DE-AC08-95NV11508 and DE-AC08-00NV13609. Approved for public release; further dissemination unlimited.

ABSTRACT

Determination of groundwater flow velocities at the Nevada Test Site is important since groundwater is the principal transport medium of underground radionuclides. However, ^{14}C -based groundwater velocities in the carbonate aquifers of the Nevada Test Site are several orders of magnitude slower than velocities derived from the Underground Test Area regional numerical model. This discrepancy has been attributed to the loss or retardation of ^{14}C from groundwater into the surrounding aquifer matrix making ^{14}C -based groundwater ages appear much older. Laboratory experiments were used to investigate the retardation of ^{14}C in the carbonate aquifers at the Nevada Test Site. Three sets of experiments were conducted evaluating the diffusion of ^{14}C into the carbonate aquifer matrix, adsorption and/or isotopic exchange onto the pore surfaces of the carbonate matrix, and adsorption and/or isotopic exchange onto the fracture surfaces of the carbonate aquifer.

Experimental results and published aquifer matrix and fracture porosities from the Lower Carbonate Aquifer were applied to a ^{14}C retardation model. The model produced an extremely wide range of retardation factors because of the wide range of published aquifer matrix and fracture porosities (over three orders of magnitude). Large retardation factors suggest that groundwater with very little measured ^{14}C activity may actually be very young if matrix porosity is large relative to the fracture porosity. Groundwater samples collected from highly fractured aquifers with large effective fracture porosities may have relatively small correction factors, while samples from aquifers with a few widely spaced fractures may have very large correction factors.

These retardation factors were then used to calculate groundwater velocities from a proposed flow path at the Nevada Test Site. The upper end of the range of ^{14}C correction factors estimated groundwater velocities that appear to be at least an order of magnitude too high compared to published velocities. The lower end of the range of ^{14}C correction factors falls within the range of reported velocities. From these results, future experimental studies (both laboratory and field scale) to support ^{14}C groundwater age dating should focus on obtaining better estimates of aquifer properties including matrix and fracture porosities.

CONTENTS

ABSTRACT.....	ii
LIST OF FIGURES	iv
LIST OF TABLES.....	iv
NOTATION.....	v
ACRONYMS.....	vii
INTRODUCTION	1
BACKGROUND	2
EXPERIMENTAL METHODOLOGY.....	7
Sample Collection and Analytical Methods	7
Diffusion Experiments.....	8
Experimental Design.....	9
Batch Experiments.....	11
Experimental Design.....	14
Fracture Experiments.....	15
Experimental Design.....	15
EXPERIMENTAL RESULTS.....	17
Diffusion Experiments.....	17
Physical Properties of the Carbonate Matrix	17
Diffusion Coefficients.....	17
Batch Experiments.....	19
Fracture Experiments.....	22
Br ⁻ Tracer Experiments.....	22
¹⁴ C Tracer Experiments.....	25
Simultaneous ¹⁴ C and Br ⁻ Experiments.....	25
DISCUSSION.....	29
Implications for ¹⁴ C Transport at Large Scales and ¹⁴ C Groundwater Dating	29
Recommendations for Future Experimental Studies to Support ¹⁴ C Groundwater Dating ..	32
CONCLUSIONS.....	33
REFERENCES	34
Appendix A: Laboratory Results of Diffusion Experiments	A-1
Appendix B: Laboratory Results of Batch Experiments.....	B-1
Appendix C: Laboratory Results of Fracture Experiments.....	C-1

LIST OF FIGURES

1. Conceptual model of important processes controlling ^{14}C activity in groundwater.....	4
2. Experiment apparatus used to measure diffusion in NTS carbonate aquifer core.....	11
3. Experimental apparatus to measure ^{14}C retardation in NTS carbonate aquifer material.....	16
4. Br^- concentration vs. $\text{time}^{1/2}$ and regression line for Cell E, Core #1.....	18
5. Br^- concentration vs. $\text{time}^{1/2}$ and regression line for Cell B, Core #2.....	18
6. Br^- concentration vs. $\text{time}^{1/2}$ and regression line for Cell F, Core #3.....	19
7. ^{14}C batch sorption data and fit of Equation (50) to the data.....	20
8. ^{13}C batch sorption data and fit of Equation (50) to the data.....	20
9. Br^- response as a function of volume in fracture experiments 2 through 5.....	23
10. Br^- experimental data and RELAP modeled fits for fracture experiments 2 through 5.....	24
11. RELAP fits to the Br^- data for Experiment 5 (0.84 mL/min).....	24
12. Br^- and ^{14}C data from Experiment 9 and RELAP fits to the data.....	26
13. Br^- and ^{14}C data from Experiment 10 and RELAP fits to the data.....	26
14. Ratio of apparent ^{14}C age to true groundwater age as a function of n_p^*/n_f for different ^{14}C K_d values.....	30
15. n_p^*/n_f for different fracture spacings and different matrix porosities (numbers on plot) assuming 1-mm aperture fractures.....	31

LIST OF TABLES

1. Physical properties of the three carbonate cores used in the diffusion experiments.....	17
2. Effective diffusivities and tortuosities of the three carbonate cores used in the diffusion experiments.....	19
3. Water chemistry of batch experiments.....	21
4. Instantaneous distribution coefficient (k_3), forward and backward rate (k_1 and k_2), and the overall distribution coefficient (K_d) obtained from the batch experiments.....	22
5. Br^- and ^{14}C fracture experiment parameters.....	22
6. RELAP model parameters providing the best simultaneous fits to the Br^- breakthrough curves (see Figure 11).....	24
7. Chemical data for ^{14}C fracture experiments.....	25
8. RELAP model parameters providing the best fits to the breakthrough curves in the two multiple tracer experiments (see Figures 12 and 13). ¹	27
9. Corrected distribution coefficients using Equation (55); overall distribution coefficients (K_d) from batch experiments; instantaneous distribution coefficients (k_3) values from fracture experiments.....	28

NOTATION

- A: cross-sectional area, L^2
- B: fitting parameter, see page 6, Equation (20) for definition
- C: concentration, M/L^3 or dpm/L^3
- C_0 : initial tracer concentration, M/L^3 or dpm/L^3
- \bar{C} : Laplace transformed dependent variable of concentration
- C_f : tracer concentration of water within the fractures, M/L^3 or dpm/L^3
- C_{final} : final tracer concentration at equilibrium for batch experiments, M/L^3 or dpm/L^3
- C_i : initial tracer concentration, M/L^3
- C_p : tracer concentration of water within the porous rock matrix, M/L^3 or dpm/L^3
- C_{rapid} : tracer concentration in solution very early in batch sorption experiments, M/L^3 or dpm/L^3
- C_{res} : reservoir concentration, M/L^3
- D_0 : free water diffusion coefficient, L^2/T
- D_m : diffusion coefficient in the matrix, L^2/T
- D_p : effective diffusion coefficient, L^2/T
- E: fitting parameter, see page 6, Equation (25) for definition
- F: mass flux of tracer, M/T
- K_d : equilibrium distribution coefficient, L^3/M
- K^*_d : corrected equilibrium distribution coefficient, L^3/M
- L: fracture spacing, L
- L_f : fracture length, L
- L_{pe} : length of core, L
- M: mass of solid in contact with solution, M
- Pe: Peclet number
- Q: volumetric flow rate through fracture, L^3/T
- R: total retardation factor, dimensionless
- R_{af} : retardation factor owing to instantaneous equilibrium adsorption on fracture surfaces
- R_{ak} : retardation factor owing to kinetic adsorption within the porous rock matrix
- R_{ap} : retardation factor owing to instantaneous equilibrium adsorption within the porous rock matrix
- S: surface concentration on solids, M/M or dpm/M
- \bar{S} : Laplace transformed dependent variable of surface concentration
- V: reservoir volume, L^3
- W: fracture width, L
- Z_a : correction factor for specific surface area as a function of matrix porosity
- Z_b : specific surface area of crushed material, L^2/M
- Z_p : specific surface area of solid matrix, L^2/M

a: fitting parameter, see page 6, Equation (19) for definition

b: half-fracture aperture, L

k_1 : forward rate constant, T^{-1}

k'_1 : reduced forward rate constant, T^{-1}

k_2 : backward rate constant, T^{-1}

k_3 : instantaneous equilibrium distribution coefficient, L^3/M

k_i : instantaneous adsorption distribution coefficient, L

m: slope of regression line

n: effective matrix porosity

n_f : fracture porosity

n_p^* : $(1-n_f) \phi$

n_p : matrix porosity

q: mass flux

q_1 : tracer concentration in the solid phase governed by instantaneous equilibrium, M/M or dpm/M

q_2 : tracer concentration in the solid phase governed by a first-order non-equilibrium kinetic reaction, M/L^2 or dpm/L^2

s: Laplace transform independent variable

t: time, T

t_a : apparent radiocarbon groundwater age, T

t_0 : true groundwater age, T

v: mean flow velocity, L/T

v' : reduced mean flow velocity, L/T

w_d : dry weight, M

w_s : saturated weight, M

x: distance along the direction of flow, L

y: distance perpendicular to fracture orientation, L

α_{pe} : dispersivity

λ : radioactive decay constant, T^{-1}

ϕ : total porosity

ϕ_1 : mass transfer of tracer between the liquid and solid phases in the matrix, governed by a linear adsorption isotherm and instantaneous equilibrium, T^{-1} or $dpmM^{-1}T^{-1}$

ϕ_2 : mass transfer of tracer between the liquid and solid phases in the matrix, governed by a non-equilibrium kinetic reaction of the first order, T^{-1} or $dpmM^{-1}T^{-1}$

ϕ_{ref} : reference porosity at which K_d values were measured

ρ_b : dry bulk density of the rock matrix material, M/L^3

ρ_d : particle density of the rock matrix material, M/L^3

ρ_{Br} : density of bromide tracer solution, M/L³

τ : tortuosity

τ_f : mean tracer residence time in fracture, T

ACRONYMS

DRI	Desert Research Institute
LCA	Lower Carbonate Aquifer
NTS	Nevada Test Site
UGTA	Underground Test Area

INTRODUCTION

Determination of groundwater flow velocities at the Nevada Test Site (NTS) is important since groundwater is the principal transport medium of underground radionuclides. However, uncorrected carbon-14 (^{14}C) based groundwater velocities in the carbonate aquifers of the NTS are several orders of magnitude slower than velocities derived from the Underground Test Area (UGTA) regional numerical model. This discrepancy has been attributed to the loss of ^{14}C from NTS groundwater by diffusion into the surrounding aquifer matrix making ^{14}C -based groundwater ages appear much older (GeoTrans, 1995; Waddell, 1984).

Conceptually, ^{14}C in groundwater flowing within the fractures of the carbonate aquifer diffuses from the fractures into the pores of the surrounding, less permeable aquifer matrix. Once in the pores, where flow is essentially negligible, ^{14}C remains until it decays. Since advective flow in the fractures is faster than diffusional flow in the matrix, ^{14}C in the fractures is continually replaced. Thus, as immobile ^{14}C in the pores decays, a ^{14}C concentration gradient develops from the fractures to the matrix. This continuous loss of ^{14}C from the active flow system produces ^{14}C groundwater ages that appear to be much older; and therefore, calculated groundwater flow velocities are much slower.

The effects of matrix diffusion as a significant process in the retardation of ^{14}C and other solutes in groundwater flow systems have been considered by numerous investigators (Gonfiantini, 1988; Maloszewski and Zuber, 1985, 1990, 1991; Neretnieks, 1980; Sudicky and Frind, 1981). Additionally, adsorption and/or ion exchange of ^{14}C onto fracture and pore surfaces may also affect ^{14}C -derived ages and velocities. Theoretical equations describing ^{14}C diffusion into an aquifer matrix and adsorption and/or ion exchange of ^{14}C onto fracture and pore surfaces have been developed. However, few laboratory or field-scale experiments have been conducted to test the validity of these models. The equations used in this study assume groundwater movement along a flowpath where groundwater recharge and mixing of different groundwater masses are not occurring.

The objective of this research is to investigate the retardation of ^{14}C in groundwater within the carbonate aquifer at the NTS. Specifically, three mechanisms of retardation are evaluated:

- diffusion of ^{14}C into the carbonate aquifer matrix;
- adsorption and/or isotopic exchange of ^{14}C onto the pore surfaces of the carbonate aquifer matrix; and,
- adsorption and/or isotopic exchange of ^{14}C onto the fracture surfaces of the carbonate aquifer.

The approach used to accomplish the objective was to design and conduct a series of laboratory experiments to quantify values for several unknown variables in previously developed retardation equations. The retardation values reported can be used to correct ^{14}C -based groundwater ages in the vicinity of the NTS since they are calculated from equations assuming a constant natural flux of ^{14}C in groundwater. However, because the amount of ^{14}C produced from underground nuclear testing will not be constant, a different model to calculate retardation of ^{14}C from nuclear testing may be required.

BACKGROUND

Considerable research has been conducted to define the important processes controlling solute transport through fractured aquifers and to develop the governing equations defining these processes. Early works include Grisak and Pickens (1980, 1981), Grisak *et al.* (1980), Neretnieks (1980), Neretnieks *et al.* (1982), Rasmuson and Neretnieks (1981), Sudicky and Frind (1982), and Tang *et al.* (1981). More recently, Maloszewski and Zuber (1985, 1990, 1991) have considered the combined effects of matrix diffusion, adsorption, and/or exchange reactions. Several of the relevant studies are described below.

Neretnieks (1980) was among the first to suggest that diffusion into the rock matrix was an important mechanism in the retardation of ^{14}C in fractured aquifers. Neretnieks concluded that the importance of diffusion is largely dependent on fracture width and spacing. Later, Rasmuson and Neretnieks (1981) demonstrated that for groundwater flowing through a granitic rock having an average fracture width of 1 mm, a fracture spacing of approximately 1 meter, and an effective matrix porosity of 0.5 percent, ^{14}C ages would be 10 to 70 times greater than the true groundwater age. For the same rock having more narrow fissures (0.01 mm), ^{14}C ages would be more than 1,000 times larger.

Sudicky and Frind (1981) examined the diffusive losses of ^{14}C into fine-grained aquitards overlying a confined aquifer. They combined several groundwater governing equations including one-dimensional steady state, advective-dispersive transport, and diffusion into an analytical model. They then chose theoretical values of typical groundwater systems for various parameters and calculated results based upon their model. They concluded that diffusion of ^{14}C into an aquitard causes a slower advance of ^{14}C resulting in apparent groundwater velocities that were much less than true flow velocities. For example, in a hypothetical aquifer, with a “true” groundwater velocity of 3.6 m/yr (^{14}C traveled 36 km in 10,000 yrs), the apparent groundwater velocity was 3.3 m/yr using a diffusion coefficient of 10^{-8} , for 10^{-7} the apparent velocity was 3.0 m/yr, for 10^{-6} the apparent velocity was 1.8 m/yr, and for 10^{-5} the apparent velocity was 0.8 m/yr.

Maloszewski and Zuber (1985) examined the importance of matrix diffusion through development of a flow and transport model to simulate tracer movement through a porous matrix containing parallel, equally spaced fractures. In long-term experiments, they found tracer movement can be significantly affected by diffusion into the porous matrix. For sorbing tracers, they concluded that adsorption would be significant because of the large surface area within the matrix. They then applied their model to the multi-tracer experiments of Garnier (1985), which had been conducted in a fissured chalk (carbonate) formation. Using Carbon-13 (^{13}C) as a tracer, it was shown that H^{13}CO_3 undergoes a strong interaction with the carbonate matrix. Lastly, it was shown that isotopic exchange may yield ^{14}C ages orders of magnitude older.

Gonfiantini (1988) noted a close relationship between ^{13}C and ^{14}C signatures in groundwater samples collected from a karst aquifer in Libya and concluded that bicarbonate within the groundwater was undergoing isotopic exchange with the carbonate bedrock. Carbon exchange was modeled as a first-order reaction described by a single kinetic rate constant (k) applicable to both isotopes. Through comparison of the ^{13}C and ^{14}C data, k was estimated to be approximately equal to half the ^{14}C decay rate (l) and therefore has a half-reaction time of roughly 11,000 years.

As an improvement on their earlier paper, Maloszewski and Zuber (1990) coupled transport equations for a single fracture with the chemical adsorption model of Cameron and Klute (1977). The revised model for the matrix includes both an instantaneous equilibrium reaction (governed by a linear adsorption isotherm) and a first-order nonequilibrium kinetic reaction. For simplicity, adsorption on the fracture walls is approximated only by an instantaneous equilibrium reaction governed by a linear adsorption isotherm. They then applied the revised model to the multi-tracer experiments of Garnier (1985). Based on curve fitting of these data, Maloszewski and Zuber (1990) concluded that their model, which accounts for matrix diffusion as well as adsorption, worked very well for non-sorbing tracers but less well for sorbable tracers. From this observation, Maloszewski and Zuber suggested that the reaction model employed in the simulations is likely to be more important than the geometry of the fracture network.

Based upon the results of their earlier work and, in particular, the conclusion that the fracture geometry does not appear to be critical, Maloszewski and Zuber (1991) combined the model of parallel fissures (Sudicky and Frind, 1982) with the adsorption model of Cameron and Klute (1977). Conceptually, the combined model consists of a dual-porosity fissured rock approximated by a semi-infinite system of identical, parallel fissures equally spaced in a porous matrix. Tracer continuously enters the aquifer with inflowing water and is transported along the fractures by groundwater. Tracer distribution across the fractures is assumed to be constant as a result of sufficient transverse dispersion. In addition, longitudinal dispersion is treated as inconsequential in comparison to the effect of radioactive decay. Lastly, it is assumed that convective flow within the matrix is negligible. Tracer retardation is seen to be a function of four processes. First, adsorption on the fissure walls may occur and is assumed to be instantaneous and governed by a linear adsorption isotherm. Secondly, the tracer may diffuse into the matrix, a process governed by the tracer concentration gradient between the fissures and the porous matrix. Once within the matrix, two other processes affect tracer concentration: an instantaneous equilibrium reaction and a first-order nonequilibrium kinetic reaction. These processes are illustrated in Figure 1.

Given these assumptions, the following one-dimensional governing equations (Maloszewski and Zuber, 1991) have been constructed. Radiocarbon transport within the fractures is described by:

$$R_{af} \frac{\partial C_f}{\partial t} + v \frac{\partial C_f}{\partial x} - \frac{n_p D_p}{b} \frac{\partial C_p}{\partial y} \Big|_{y=b} + \lambda R_{af} C_f = 0 \quad (1)$$

where R_{af} is the retardation factor owing to instantaneous adsorption of radiocarbon onto the fracture walls, C_f is the ^{14}C signature of water within the fractures, and C_p is the ^{14}C signature of water within the matrix, t represents time, v is the mean water velocity within the fractures, x is the direction of flow within the fractures, n_p is the matrix porosity, D_p is the effective molecular diffusion coefficient for ^{14}C , b represents the half-fracture aperture, y is the direction perpendicular to the fracture orientation, and λ represents the decay constant of ^{14}C ($1.4\text{E-}08 \text{ hours}^{-1}$).

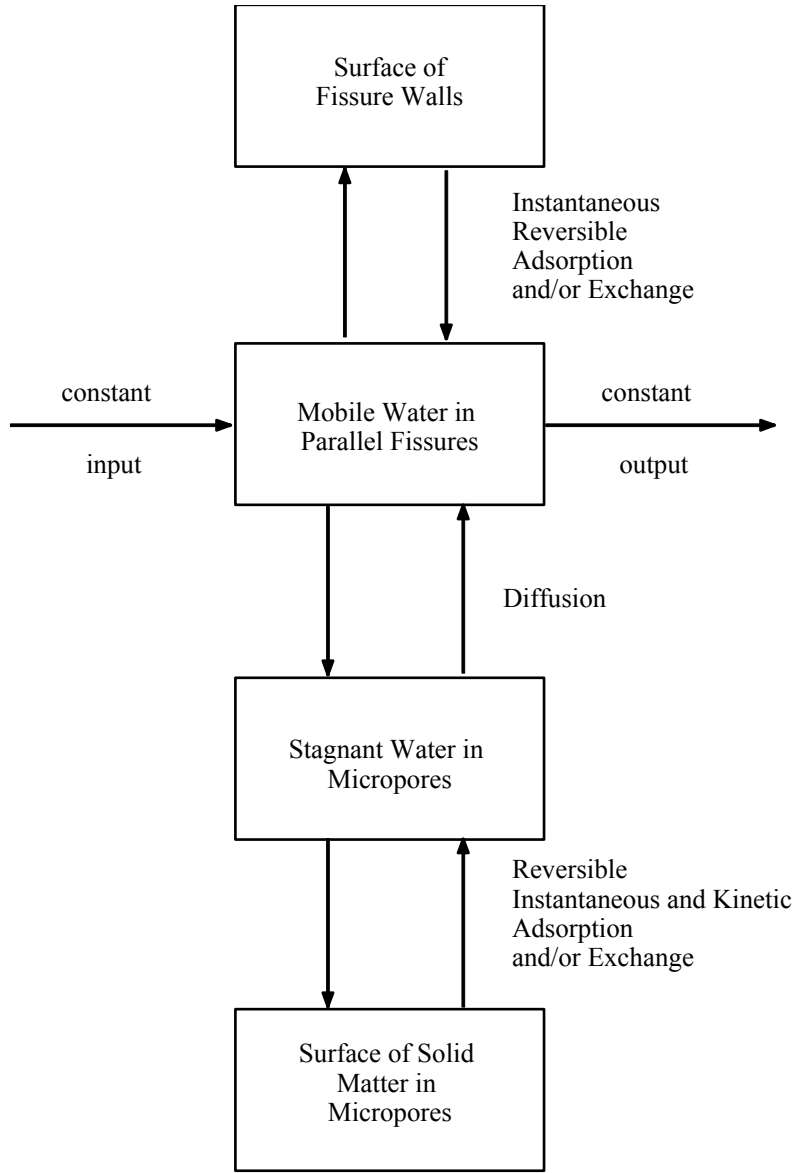


Figure 1. Conceptual model of important processes controlling ^{14}C activity in groundwater (from Maloszewski and Zuber, 1991).

Carbon-14 transport within the matrix is given by:

$$n_p \frac{\partial C_p}{\partial t} + (1 - n_p) \rho_d (\phi_1 + \phi_2) - n_p D_p \frac{\partial^2 C_p}{\partial y^2} + \lambda n_p C_p = 0 \quad (2)$$

where ρ_d represents the particle density of the matrix material, and ϕ_1 and ϕ_2 represent mass transfers of ^{14}C between the liquid and solid phases in the matrix. ϕ_1 is governed by a linear

adsorption isotherm and instantaneous equilibrium whereas ϕ_2 is governed by a non-equilibrium reaction of the first order. The two mass transfer parameters are defined by:

$$\phi_1 = \frac{\partial q_1}{\partial t} + \lambda q_1 = k_3 \frac{\partial C_p}{\partial t} + \lambda k_3 C_p \quad (3)$$

$$\phi_2 = \frac{\partial q_2}{\partial t} + \lambda q_2 = \frac{k_1 n_p C_p}{(1 - n_p) \rho_d} - k_2 q_2 \quad (4)$$

where q_1 is the partial tracer concentration in the solid phase governed by instantaneous equilibrium and q_2 is the partial tracer concentration in the solid phase governed by non-equilibrium kinetic reactions, k_3 is the distribution constant for an instantaneous equilibrium, and k_1 and k_2 are the forward and backward rate constants for the non-equilibrium kinetic reaction. By defining the following:

$$v' = \frac{v}{R_{af}} \quad (5)$$

$$R_{ap} = 1 + (1 - n_p) \rho_d \frac{k_3}{n_p} \quad (6)$$

where R_{ap} represents the retardation factor attributable to the instantaneous reaction in the matrix, and then combining Equations (1) through (4), the governing equations can be re-written as:

$$\frac{\partial C_f}{\partial t} + v' \frac{\partial C_f}{\partial x} - \frac{n_p D_p}{b R_{af}} \frac{\partial C_p}{\partial y} \Big|_{y=b} + \lambda C_f = 0 \quad (7)$$

$$R_{ap} \frac{\partial C_p}{\partial t} + \lambda R_{ap} C_p + \frac{1 - n_p}{n_p} \rho_d \left(\frac{\partial q_2}{\partial t} + \lambda q_2 \right) - D_p \frac{\partial^2 C_p}{\partial y^2} = 0 \quad (8)$$

$$\frac{dq_2}{dt} = k_1 \frac{n_p C_p}{(1 - n_p) \rho_d} - k_2 q_2 - \lambda q_2 = 0 \quad (9)$$

The following boundary and initial conditions are defined:

$$C_f(x, 0) = 0 \quad (10)$$

$$C_f(0, t) = C_0 \quad (11)$$

$$C_f(\infty, t) = 0 \quad (12)$$

$$C_p(y, x, 0) = 0 \quad (13)$$

$$C_p(b, x, t) = C_f(x, t) \quad (14)$$

$$\frac{\partial C_p}{\partial y} \Big|_{y=L/2} = 0 \quad (15)$$

$$q_1(y, x, 0) = 0 \quad (16)$$

$$q_2(y, x, 0) = 0 \quad (17)$$

where L represents fracture spacing and C_0 is the initial tracer concentration. Applying Laplace transforms to Equations (7) through (9) and making use of the initial and boundary conditions, the following equation is obtained:

$$\frac{C_f(\infty)}{C_0} = \exp \left\{ -\lambda R_{af} t_0 \left[1 + \left(\frac{2aB}{\lambda^{1/2}} \right) \cdot \tanh \left(\frac{R_{ap} \lambda^{1/2} n_p (1 - n_f) B}{2R_{af} a n_f} \right) \right] \right\} \quad (18)$$

where t_0 is the true groundwater age and the the following parameters are defined by:

$$a = \frac{n_p (D_p R_{ap})^{1/2}}{2bR_{af}} \quad (19)$$

$$B = \left[\frac{k'_1 + k_2 + \lambda}{k_2 + \lambda} \right]^{1/2} \quad (20)$$

$$n_f = \frac{2b}{L} \quad (21)$$

$$k'_1 = \frac{k_1}{R_{ap}} \quad (22)$$

If the fracture porosity (n_f) is much less than unity, and if the backward rate constant (k_2) is much greater than the radioactive decay constant, Equation (18) can be approximated as:

$$\frac{C_f(\infty)}{C_0} = \exp \left\{ -\lambda R_{af} t_0 \left[1 + \frac{2a(1 + \frac{k'_1}{k_2})^{1/2}}{\lambda^{1/2}} \tanh(E) \right] \right\} \quad (23)$$

where

$$1 + \frac{k'_1}{k_2} = \left(\frac{R_{ap} + \frac{k_1}{k_2}}{R_{ap}} \right) \quad (24)$$

$$E = n_p \left[\frac{\lambda R_{ap} (R_{ap} + R_{ak})^{1/2}}{2R_{af} a n_f} = b \frac{\lambda (R_{ap} + R_{ak})^{1/2}}{D_p^{1/2} n_f} \right] \quad (25)$$

and where

$$R_{ak} = \frac{k_1}{k_2} \quad (26)$$

is the retardation factor caused by the kinetic reaction in the matrix. Comparing Equation (23) to the radioactive decay formula:

$$\frac{C_f(x, \infty)}{C_0} = \exp(-\lambda t_a) \quad (27)$$

where t_a represents the apparent radiocarbon age, the following expression may be utilized to correct the radiocarbon age of a groundwater sample to the true age of the water (t_0):

$$\frac{t_a}{t_0} = R = \left\{ R_{af} \left[1 + \frac{2a \frac{R_{ap} + R_{ak}^{1/2}}{R_{ap}}}{\lambda^{1/2}} \tanh(E) \right] \right\} \quad (28)$$

EXPERIMENTAL METHODOLOGY

Sample Collection and Analytical Methods

A series of laboratory experiments was designed using carbonate aquifer material from the NTS to examine the important radiocarbon retardation processes described above. The goal was to generate values that can be used in Equation (28) to solve for the total retardation of ^{14}C in NTS groundwater. In addition, the behavior of ^{13}C relative to ^{14}C was examined in preparation for a field-scale experiment that would use ^{13}C as an analog to ^{14}C . Groundwater was collected from Army #1 Water Well on July 2, 1997 after pumping the well for two hours. Samples were collected in one-liter glass bottles and shipped to the Desert Research Institute (DRI), Reno, Nevada. Lower Carbonate Aquifer (LCA) core from UE-7nS and Army #1 Water Well were selected from the NTS Core Library on June 5, 1997 and shipped to the DRI in Reno for the experiments. Permission to use the cores was granted by Lawrence Livermore National Laboratory (UE-7nS) and the U. S. Geological Survey (Army #1 Water Well).

Samples for ^{14}C analysis were analyzed at the DRI's Analytical Chemistry Laboratory in Reno. One-mL water samples were combined with 10 mL of Ecolite scintillation cocktail and were analyzed with a Beckman Liquid Scintillation Spectrometer. Samples for ^{13}C analysis were analyzed at DRI's Environmental Isotope Laboratory, in Las Vegas, Nevada. The ^{13}C samples were first treated with strontium chloride and sodium hydroxide to precipitate dissolved carbon. The precipitated carbon was then converted to CO_2 gas by acid hydrolysis using phosphoric acid and analyzed in a Finnigan Model Delta-E Mass Spectrometer. All other chemical analyses were conducted at the DRI's Analytical Chemistry Laboratory in Reno. pH was measured using a Beckman pH meter and alkalinity was determined by manual titration to the pH 4.5 endpoint using sulfuric acid under an exhaust hood to minimize exposure of laboratory personnel to residual ^{14}C in the samples. Ca^{2+} and Mg^{2+} were analyzed on an Instructions Atomic Absorption Spectrometer, while Br^- was analyzed with either a Dionex Ion Chromatograph or an ion-specific probe.

Diffusion Experiments

Solutes in a solution, including ^{14}C in groundwater, naturally move from areas of high concentration to those of low concentration because of Brownian motion, a process known as molecular diffusion, or simply diffusion. Diffusion may occur in both free liquid or in flowing groundwater within an aquifer, provided that a concentration gradient exists. The mass flux, q , of solute diffusing through a given cross section of the aquifer matrix per unit time is proportional to the concentration gradient, as expressed by Fick's First Law:

$$q = -D_p n \frac{\partial C}{\partial x} \quad (29)$$

where

$$D_p = D_0 \tau \quad (30)$$

and $\partial C/\partial x$ is the one-dimensional concentration gradient in the x direction, n is the effective porosity of the rock matrix, D_p represents the effective diffusion coefficient within the rock for a specific solute, D_0 is the diffusion coefficient for the same solute in a free solution, and τ describes the tortuosity of the pore channels through which the solute diffuses.

The effective diffusion coefficient, D_p , for ^{14}C in the carbonate aquifer matrix of the NTS was estimated using methodology developed by Tyler (personal communication, DRI, 1997). This method is advantageous over other techniques because the sample to be tested remains intact, analysis is relatively rapid and straightforward, and the measuring apparatus is simple to construct. The method utilizes the diffusive transport equation (assuming no sorption and an independence of D_p with concentration):

$$\frac{\partial C}{\partial t} = \frac{D_p \partial^2 C}{\partial x^2} \quad (31)$$

which is solved using prescribed initial and time-invariant (Dirichlet) boundary conditions. A rock core saturated with a solute having an initial solute concentration C_i is placed in contact with a large reservoir of water having an initial solute concentration C_{res} . Within the reservoir, solute concentration will slowly rise as the solute diffuses out of the rock core. However, if the reservoir volume is much greater than the pore volume of the core and if $C_i \gg C_{\text{res}}$, changes in reservoir concentration will be small compared to C_i . Concentration changes at the boundary then are insignificant and the concentration gradient can be treated as a constant. Furthermore, if the core is sufficiently long, solute concentration at the closed end of the core can be assumed to remain at its initial concentration throughout the experiments.

Given that the initial and boundary conditions have been met, the solution to the diffusive transport equation is:

$$C_{\text{res}} = C_i \operatorname{erf} \left[\frac{x}{2\sqrt{D_p t}} \right] \quad (32)$$

where erf is the error function. The concentration gradient at any point along the sample is found by taking the partial derivative of Equation (32) with respect to x , yielding:

$$\frac{\partial C_{\text{res}}}{\partial x} = \frac{C_i \exp\left[-\frac{x^2}{4D_p t}\right]}{\sqrt{\pi D_p t}} \quad (33)$$

Evaluating Equation (33) at $x = 0$ (the sample/reservoir interface) and then substituting the result back into Equation (29) provides an expression describing the mass flux of solute per unit area of core across the interface (in the negative x direction):

$$q(0, t) = C_i n \frac{\sqrt{D_p}}{\sqrt{\pi t}} \quad (34)$$

The mass flux out of the core must be accompanied by an equivalent gain in solute within the reservoir:

$$VC_{\text{res}} = A \int_0^t q \partial t = \frac{AC_i n \sqrt{D_p}}{\sqrt{\pi}} \int_0^t t^{-1/2} \partial t \quad (35)$$

where V is the volume of the reservoir and A is the cross-sectional area of the core. Integrating gives:

$$VC_{\text{res}} = \frac{2AC_i n \sqrt{D_p}}{\sqrt{\pi}} t^{1/2} \quad (36)$$

The above equation may be easily employed to determine the effective diffusion coefficient of a given solute in a core. One end of a core sample, previously saturated with a known concentration of the solute in question, is brought into contact with a large reservoir of water having a low concentration of the same solute. Samples from the well-stirred reservoir fluid (of sufficiently low volume to cause negligible change to the reservoir volume) are then collected over time and analyzed in the laboratory. By plotting C_{res} vs. $t^{1/2}$, the effective diffusion coefficient can be easily calculated from the slope (m) of the regression line passing through the data points and a form of Equation (36) re-arranged to:

$$\frac{C_{\text{res}}}{t^{1/2}} = m = \left(\frac{2A}{V}\right) \frac{C_i n \sqrt{D_p}}{\sqrt{\pi}} \quad (37)$$

Experimental Design

Three rock cores, each approximately 1.9 cm in diameter, were drilled from a 7.6-cm-diameter carbonate core that had been collected from the saturated zone of well UE-7nS at a depth interval of 643.1 to 643.4 m below ground surface. Upon collection, the three cores were baked in an oven at 105°C for 24 hours and the dry weight (w_d) of each core was measured. A small fraction of the initial core was also collected for particle density (ρ_d) determination using the Pycnometer Method (Klute, 1986). Thereafter, the bulk density (ρ_b) and total porosity (ϕ) of the core were estimated from:

$$\rho_b = \frac{w_d}{V} \quad (38)$$

$$\phi = 1 - \frac{\rho_b}{\rho_d} \quad (39)$$

where V represents the total volume of an individual core. For comparison, a fragment of the original rock core was also sent to Micromeritics, Inc. for porosity determination using mercury intrusion porosimetry.

The three cores were then placed in a shallow volume of 1,000 mg/L LiBr solution under vacuum to induce saturation in each core. ^{14}C could not be used as a tracer directly because of the possibility of adsorption and/or isotopic exchange. The Br^- was assumed to behave conservatively, *i.e.* not affected by adsorption and/or isotopic exchange. Potentially, the Br^- does not behave conservatively because the pH of the LiBr plus distilled water solution is 6.3, which is below the point of zero surface charge for a suspension of CaCO_3 in equilibrium with air (approximately pH 8.6; Stumm and Morgan, 1996). Using this solution, at this pH, would produce a net positive charge on the calcite surfaces; thus allowing some Br^- to adsorb onto the calcite surfaces. However, because the porosity of the cores is very low, and because a high concentration of Br^- was used, it is assumed that the high concentration of Br^- would easily “swamp” the available adsorption sites, allowing ample Br^- to diffuse into and out of the cores. The cores were periodically removed from the saturation chamber for weighing. The saturation process continued until no change in mass occurred over a period of more than six weeks. Assuming complete saturation, the effective porosity (n) of a core can be calculated from:

$$n = \frac{(w_s - w_d)}{\rho_{\text{Br}} V} \quad (40)$$

where w_s is the saturated mass of the core and ρ_{Br} represents the density of the Br^- tracer solution, assumed to be equal to 1 gm/cm^3 .

Diffusion experiments were conducted in diffusion cells (Figure 2) constructed from one-liter glass jars having a tight-fitting, screw-type lid. Each lid was equipped with a rubber septum for sampling. The core sample was attached to a threaded rod and suspended into the underlying solution. Lids were sealed with silicon vacuum grease to ensure a tight fit and to minimize the possibility of evaporation. The threaded rod allows the height of each core to be adjusted to maintain constant contact with the underlying reservoir of distilled water (250 mL). Cell F had a smaller volume of distilled water (190 mL) to accommodate a longer rock core. Each cell was fitted with a 15-cm-long, 18-gauge needle, permanently placed through the rubber septum, which was used to collect 1-mL samples of reservoir solution. Throughout the diffusion experiments, the diffusion cells were set upon a vibrating platform, which was operated for 15 minutes daily to keep the reservoir well mixed. The average laboratory temperature during the experiments was $21.5^\circ\text{C} \pm 3.0$.

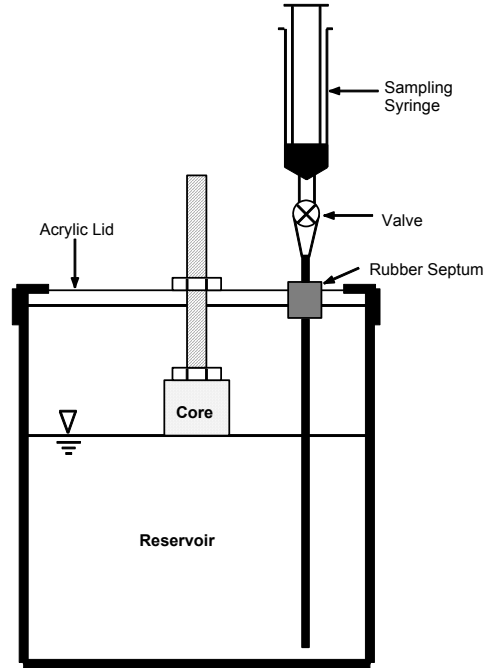


Figure 2. Experiment apparatus used to measure diffusion in NTS carbonate aquifer core.

Prior to beginning the diffusion experiments, the outer surface of each core was sealed with three coats of Varathane finish to ensure that the Br^- tracer could diffuse only through the end of the core. To ensure that all boundary conditions were met, the minimum core length (L) and maximum core area/reservoir volume ratio (A/V) were calculated from equations given by Tyler (personal communication, DRI, 1997):

$$L \geq 2(D_p t)^{1/2} \text{erf}^{-1}(0.99) \quad (41)$$

$$\frac{A}{V} \leq \frac{1}{2}(0.01) \left[\frac{n^2 D_p}{\pi} \right]^{1/2} t^{-1/2} \quad (42)$$

and compared to those utilized in the experimental design. Reservoir samples were collected from the diffusion cells over a period of five weeks and were analyzed on an ion chromatograph with a detection limit of 0.01 mg/L. Sample blanks were collected at the beginning of each experiment.

Batch Experiments

^{14}C in groundwater at the NTS exists primarily as the anion $\text{H}^{14}\text{CO}_3^-$. When $\text{H}^{14}\text{CO}_3^-$ diffuses from groundwater within a fracture into the surrounding porous matrix, reactions may occur with the grain surfaces that make up the pore walls. Assuming that the groundwater within the matrix is in chemical equilibrium with the grain surface minerals (calcite and dolomite), a minimal amount of dissolution and precipitation will occur and the $\text{H}^{14}\text{CO}_3^-$ concentration should be unaffected. Thus, over short time periods, the only processes affecting dissolved ^{14}C activity in the pore water should be adsorption and/or isotopic exchange. Evaluating the effects of each

process individually is beyond the scope of these experiments. However, the net effect of the two processes together on ^{14}C loss in the pores is considered.

Maloszewski and Zuber (1990, 1991) adopt the combined equilibrium and kinetic adsorption model of Cameron and Klute (1977). If this model is assumed to apply to the batch sorption experiments, the following approach can be taken to interpret the experiments. First, the K_d value associated with rapid equilibrium sorption (designated k_3 here) can be obtained from the standard expression used to interpret batch sorption experiments:

$$k_3 = \frac{(C_0 - C_{\text{rapid}}) V}{C_{\text{rapid}} M} \quad (43)$$

where, C_0 = initial concentration in solution, dpm/mL; C_{rapid} = concentration in solution very early in the batch sorption test (after a brief contact time between solid and solution), dpm/mL; V = volume of solution, mL; and M = mass of solid in contact with solution, g. Rearrangement of Equation (43), with the recognition that $V/M = \phi/\rho_b$ (ρ_b = effective bulk density of solid) yields:

$$C_{\text{rapid}} = \frac{C_0}{\left(1 + \frac{\rho_b}{\phi} k_3\right)} \quad (44)$$

C_{rapid} can now be considered the initial concentration for the kinetic phase of the batch sorption experiment. The equations describing this phase are:

$$\frac{dC}{dt} = -k_1 C + k_2 S \quad (45)$$

$$\frac{\rho_b}{\phi} \frac{dS}{dt} = k_1 C - k_2 S \quad (46)$$

where, S = surface concentration on solids, dpm/g; k_1 = forward rate constant, 1/day and k_2 = reverse rate constant, g/mL-day.

The Laplace transforms of Equations (45) and (46) are:

$$s\bar{C} - C_{\text{rapid}} = -k_1 \bar{C} + k_2 \bar{S} \quad (47)$$

$$\frac{\rho_b}{\phi} s \bar{S} = k_1 \bar{C} - k_2 \bar{S} \quad (48)$$

where, s = Laplace transform independent variable

\bar{C} = Laplace transformed dependent variable, concentration

\bar{S} = Laplace transformed dependent variable, surface concentration.

Solving Equation (48) for \bar{S} and substituting the result into Equation (47), and then solving for \bar{C} yields:

$$\bar{C} = \frac{C_{\text{rapid}}}{\left(s + k_1 - \frac{k_1 k_2}{\left(\frac{\rho_b}{\phi} s + k_2 \right)} \right)} \quad (49)$$

Finally, substituting Equation (44) into Equation (49) yields:

$$\bar{C} = \frac{C_0}{\left(1 + \frac{\rho_b}{\phi} k_3 \right) \left(s + k_1 - \frac{k_1 k_2}{\left(\frac{\rho_b}{\phi} s + k_2 \right)} \right)} \quad (50)$$

The time-domain solution to Equation (50) can be obtained by numerically inverting the Laplace-domain equation using an inversion method such as that used by Reimus and Haga (1999, Appendix B). The inverted solution can then be fitted to the batch sorption data by adjusting k_1 , k_2 , and k_3 to match the data.

Because the decay of ^{14}C should be very slow compared to its sorption and desorption rates, it is of practical interest to obtain the overall K_d value that describes the combined equilibrium and kinetic sorption. From batch testing, the overall K_d value is given by:

$$K_d = \frac{(C_0 - C_{\text{final}}) V}{C_{\text{final}} M} \quad (51)$$

where, C_{final} = final concentration reached after allowing sufficient time for the kinetic reaction to reach equilibrium.

The overall K_d value can be related to the constants k_1 , k_2 , and k_3 as follows. If we use

$$C_{\text{rapid}} = \frac{C_0}{\left(1 + \frac{\rho_b}{\phi} k_3 \right)}$$

as C_0 for the kinetic sorption phase, and we assume that sufficient time is

allowed to reach equilibrium, then it follows from Equation (44) that the final concentration in the batch experiment will be equal to:

$$C_{\text{final}} = \frac{C_{\text{rapid}}}{\left(1 + \frac{\rho_b}{\phi} \frac{k_1}{k_2}\right)} = \frac{C_0}{\left(1 + \frac{\rho_b}{\phi} k_3\right) \left(1 + \frac{\rho_b}{\phi} \frac{k_1}{k_2}\right)} \quad (52)$$

where k_1/k_2 is the effective equilibrium constant for the kinetic reaction.

If we substitute the right-hand side of Equation (52) into Equation (51) and rearrange, we obtain

$$K_d = k_3 + \frac{k_1}{k_2} + \frac{\rho_b}{\phi} k_3 \frac{k_1}{k_2} \quad (53)$$

Experimental Design

Batch experimental procedures were based upon similar experiments conducted by Mozeto *et al.* (1984a,b). Batch experiments were conducted using groundwater from Army #1 Water Well and carbonate core from Army #1 Water Well and UE-7nS. Cores obtained from the two wells were crushed, mixed together, and then sieved to identify the size fractions. Approximately 80 percent of the carbonate material utilized in the batch reactors was from Army #1 Water Well, while 20 percent was from UE-7nS. The size fractions ranged from 61 to 425 μm with 26 percent between 75 to 125 μm and 34 percent between 250 to 355 μm making up the largest portion. Batch reactors consisted of 250-mL glass containers with 90 grams of crushed carbonate material and approximately 180 mL of Army #1 Water Well groundwater. The carbonate material and groundwater within the batch reactors was allowed to “age” for 45 days before the batch experiments were conducted. Aging of the carbonate material allowed dissolution/precipitation reactions between the Army #1 Water Well groundwater, atmospheric CO_2 , and the crushed carbonate material to occur until equilibrium was reached. Because aged crystal surfaces are thermodynamically more stable than fresh surfaces (Mozeto *et al.*, 1984a,b), minimal loss of ^{13}C and ^{14}C tracer to carbonate mineral precipitation should occur during the batch experiments.

After 45 days of aging, the batch reactors were spiked with 22.2 mL of a solution containing 47.7 kilobecquerels/gram of solution of ^{14}C as Na_2CO_3 , producing an initial concentration in the batch reactors of 360 disintegration per minute per milliliter (dpm/mL). Additionally, the batch reactors were spiked with 11.1 mL of a solution containing ^{13}C as Na_2CO_3 , which was prepared by adding 0.8 grams of Na_2CO_3 containing 99 percent ^{13}C to 5 mL of distilled water. Addition of the ^{13}C tracer produced an initial concentration of approximately 3,400 per mil in the batch reactors. Preparation and handling of batch reactors were conducted in a glove box under nitrogen atmosphere to minimize isotopic exchange between batch reactors and CO_2 in the atmosphere. For early time experiments (^{14}C activity only), batch reactors were mixed by hand by shaking the reactor after spiking and then extracting 1.0 mL of solution with a syringe. Solid particles were removed by pushing the sample in the syringe through a 0.45- μm syringe filter and into a scintillation vial. Later time experiments were mixed by hand by shaking the reactors and then filtering through a 0.45- μm filter under nitrogen pressure. Following filtration of the later time experiments, a 1.0-mL sample was collected for ^{14}C analysis, 100-mL

sample was collected for $\delta^{13}\text{C}$ analysis and periodically a 60-mL sample was collected for analysis for pH, HCO_3^- , Ca^{2+} , and Mg^{2+} . Batch reactors for later time experiments were mixed by hand by shaking on a daily basis. Blanks consisting of Army #1 Water Well water without carbonate material were also prepared. Experiments were conducted at an average laboratory temperature of $18.6^\circ\text{C} \pm 3.7$.

Fracture Experiments

Carbon-14 in groundwater flowing through a fracture may potentially be retarded by adsorption and/or isotopic exchange of $\text{H}^{14}\text{CO}_3^-$ onto the fracture walls. To quantify this process, a series of experiments were conducted using conservative and non-conservative tracers passed through an individual fracture in a LCA core. RELAP, a computer model developed at Los Alamos National Laboratory for simulating sorbing and non-sorbing tracer transport through a dual-porosity system (Reimus and Haga, 1999, Appendix B) was used to analyze the fracture experiment data. In RELAP, flow is assumed to occur in parallel-plate fractures that are separated by a matrix containing stagnant water in its pores. One-dimensional advective-dispersive transport is assumed to occur within the fractures, and one-dimensional diffusive mass transport, perpendicular to the fracture orientation, is assumed to occur in the matrix. RELAP obtains a best least-squares fit to the time-concentration data by adjusting one or more parameters, including the mean residence time, the Peclet number ($\text{Pe} = L_{\text{Pe}}/\alpha_{\text{Pe}}$, where L_{Pe} is the core length, and α_{Pe} is the dispersivity), and a lumped parameter, $\frac{\phi}{b}\sqrt{D_m R_{\text{ap}}}$ (where b = fracture half-aperture, cm, D_m = diffusion coefficient in matrix, and R_{ap} = retardation factor in matrix), that accounts for diffusive mass transfer between the fracture and matrix and sorption in the matrix. Up to four experimental data sets can be fit simultaneously subject to logical constraints (*e.g.*, residence times are proportional to 1/flow rate, and Pe and $\frac{\phi}{b}\sqrt{D_m R_{\text{ap}}}$ are the same for all data sets) to obtain a set of parameter values that best explains all of the data.

Experimental Design

A limestone core from the saturated zone of Army #1 Water Well (390.1 to 396.5 m below ground surface) was selected. A 7.6-cm diameter and 12.4-cm-length section with a single visible fracture running the length of the section was utilized in the experiments. By visual inspection, the fracture was partially filled with white and gray crystals, most likely calcite or dolomite. The matrix porosity of a sample of the core was 6.6 percent measured by mercury intrusion porosimetry by Micromeritics Instrument Corp. Groundwater from Army #1 Water Well was spiked with Br^- (conservative) and ^{14}C (non-conservative) tracers and injected into the fracture. Br^- is assumed to behave conservatively in the limestone core at the solution pH of approximately 8.5.

To ensure that the tracers would travel only through the fracture, the surface of the core was sealed with three coats of Varathane sealant and larger openings, including vugs, were filled with epoxy. The core was then mounted between two stainless steel end plates (with openings to allow tracer to pass through), covered with shrink-wrap plastic tubing, and emplaced within a stainless steel high pressure chamber (Figure 3). The pressure chamber was utilized to apply a constant confining pressure to the exterior of the core using tap water circulated through a bladder pump. The confining pressure helped to keep the fracture aperture constant during an

experiment. Prior to starting the experiments, several liters of unspiked Army #1 Water Well water were mixed with thymol to minimize algal and bacterial growth within the core and circulated through the core to saturate the fracture. Then, several liters of fresh unspiked Army #1 Water Well water were flushed through the core to remove any remaining thymol. To start the experiment, a two-way valve was used to switch from the unspiked water to the tracer solution. To assess chemical equilibrium, samples were collected before and after each experiment and analyzed for pH, HCO_3^- , Ca^{+2} , and Mg^{+2} .

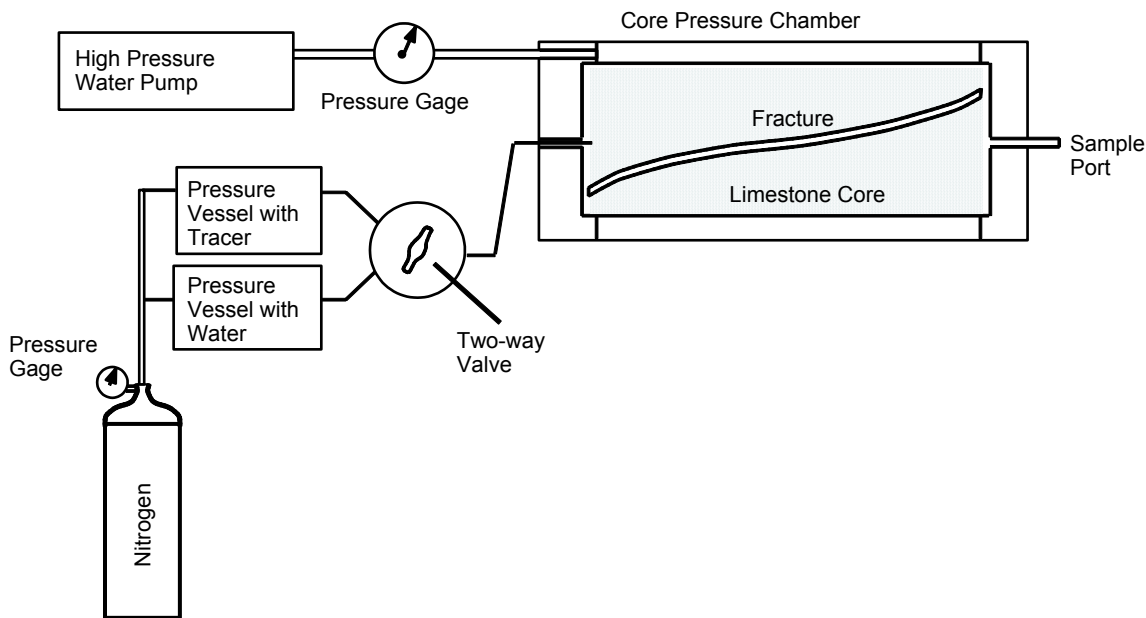


Figure 3. Experimental apparatus to measure ^{14}C retardation in NTS carbonate aquifer material.

Nine separate fracture experiments were conducted. Four of the experiments were conducted using Br^- as a single tracer and three were conducted using ^{14}C . In these experiments, a short pulse of known volume of tracer (10 mL) was used. In the remaining two experiments, Br^- and ^{14}C were injected into the fracture simultaneously for much longer duration. Flow rates were relatively fast to minimize matrix diffusion in the experiments to isolate the effects of adsorption and/or isotopic exchange on the fracture surfaces (R_{af}). In the single tracer experiments, samples were collected from a sampling port located at the end of the pressure chamber. In the dual tracer experiments, ^{14}C samples were collected and analyzed as described above. For these experiments, Br^- concentrations were read every five seconds using an inline Orion Br^- selective probe located at the outlet of the pressure chamber.

EXPERIMENTAL RESULTS

Diffusion Experiments

Physical Properties of the Carbonate Matrix

The physical properties of the carbonate cores used in the diffusion experiments (UE-7nS) were determined using measured dimensions of the drilled cores and laboratory analysis of both whole rock fragments and crushed samples of the carbonate matrix. Pycnometer analysis of approximately 25 grams of crushed carbonate produced a particle density (ρ_d) of 2.69 g/cm³. This value is somewhat less than calcite (2.72 g/cm³) and dolomite (2.85 g/cm³), indicating the presence of other, less dense minerals such as quartz (2.65 g/cm³) and k-feldspar (Hurlburt and Klein, 1977). The length and diameter of each core was then measured using a micrometer and recorded to the nearest 0.001 inch. From these measurements, the overall cross-sectional area (A) and volume (V) of each core were calculated. The bulk density (ρ_b) of the matrix was then computed using Equation (38), knowing the dry weight (w_d) and volume (V) of each of the three cores. The average bulk density for the three cores was 2.60 g/cm³. The total porosity (ϕ) of the carbonate matrix was estimated at 3.35 percent using Equation (39). Effective porosities (n) ranged from 1.70 to 2.56 percent using Equation (40) and the saturated and dry weights of each core. Results are summarized in Table 1.

Table 1. Physical properties of the three carbonate cores used in the diffusion experiments.

Core	Length (cm)	Area (A) (cm ²)	Dry Wt. (w_d) (g)	Volume (V) (cm ³)	ρ_b (g/cm ³)	Sat. Wt. (w_s) (g)	n (%)
#1	10.970	2.875	81.55	31.54	2.59	82.10	1.74
#2	10.249	2.877	77.02	29.49	2.61	77.52	1.70
#3	11.681	2.844	86.68	33.22	2.61	87.53	2.56

Particle Density (ρ_d) = 2.69 g/cm³, Total Porosity (ϕ) = 3.35 %

Diffusion Coefficients

Bromide concentration data from the diffusion experiments are listed in Appendix 1 and are illustrated in Figures 4 through 6. Results of the regression analysis for the concentration versus time data, calculated effective diffusion coefficients (D_p) for Br⁻ and for ¹⁴C, and tortuosity (t) values are listed in Table 2. The effective diffusion coefficient for Br⁻ was calculated using Equation (42) and the slope of the regression line. The tortuosity of the rock matrix for each core was then determined using Equation (30), the experimentally determined value of D_p for Br⁻, and the free water diffusion coefficient for Br⁻ ($D_0 = 2.08E-05$ cm²/sec, Klute, 1996). The effective diffusion coefficient for ¹⁴C was then calculated using Equation (30), given the calculated tortuosity values from the cores and the published free water diffusion coefficient for HCO₃⁻ ($D_0 = 1.19E-05$ cm²/sec, Klute, 1996). The effective diffusion coefficient, D_p , for ¹⁴C ranged from 2.98E-06 to 3.93E-06 cm²/sec.

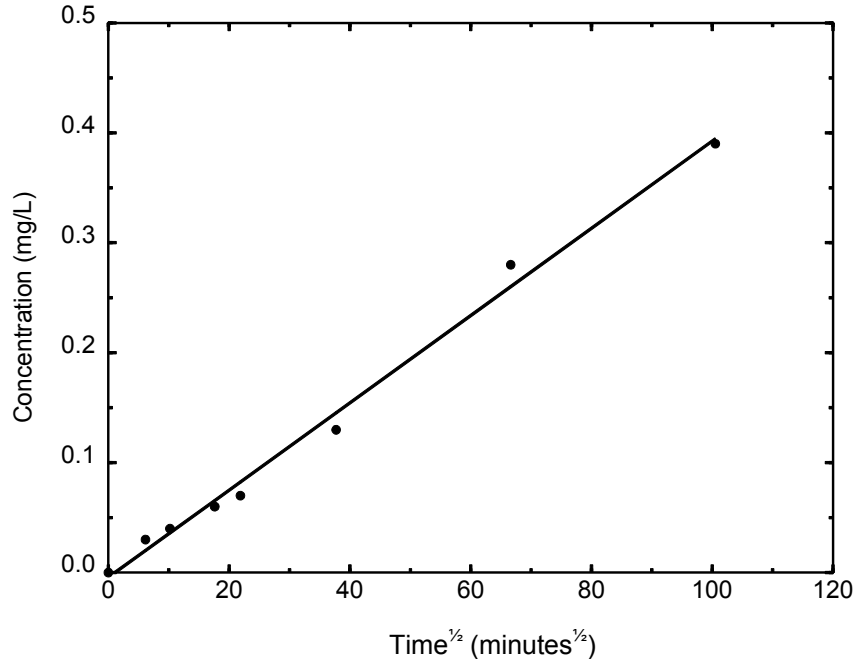


Figure 4. Br⁻ concentration vs. time^{1/2} and regression line for Cell E, Core #1.

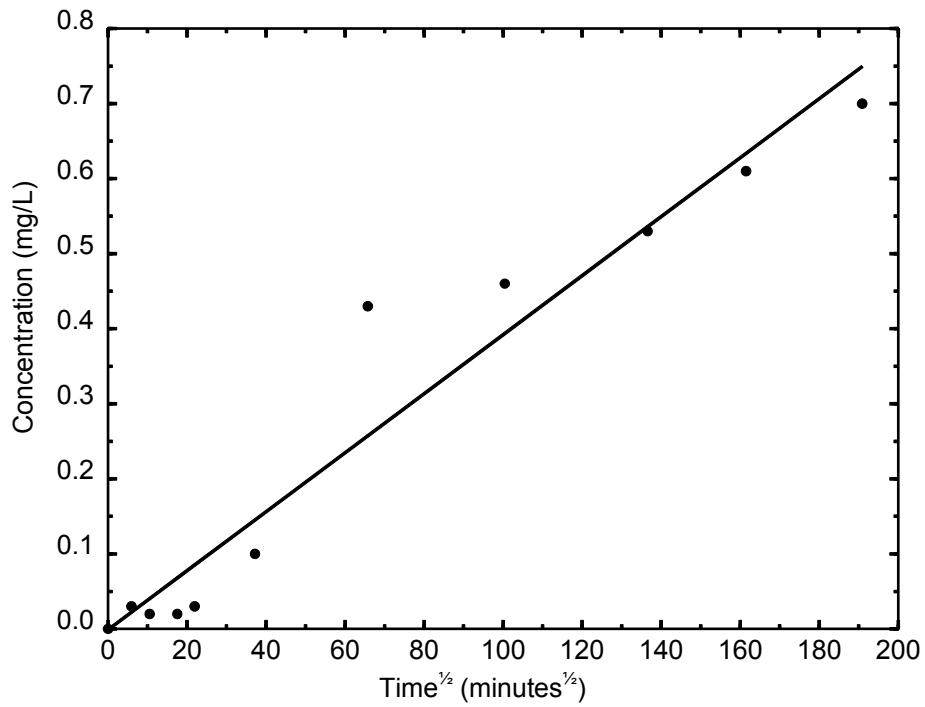


Figure 5. Br⁻ concentration vs. time^{1/2} and regression line for Cell B, Core #2.

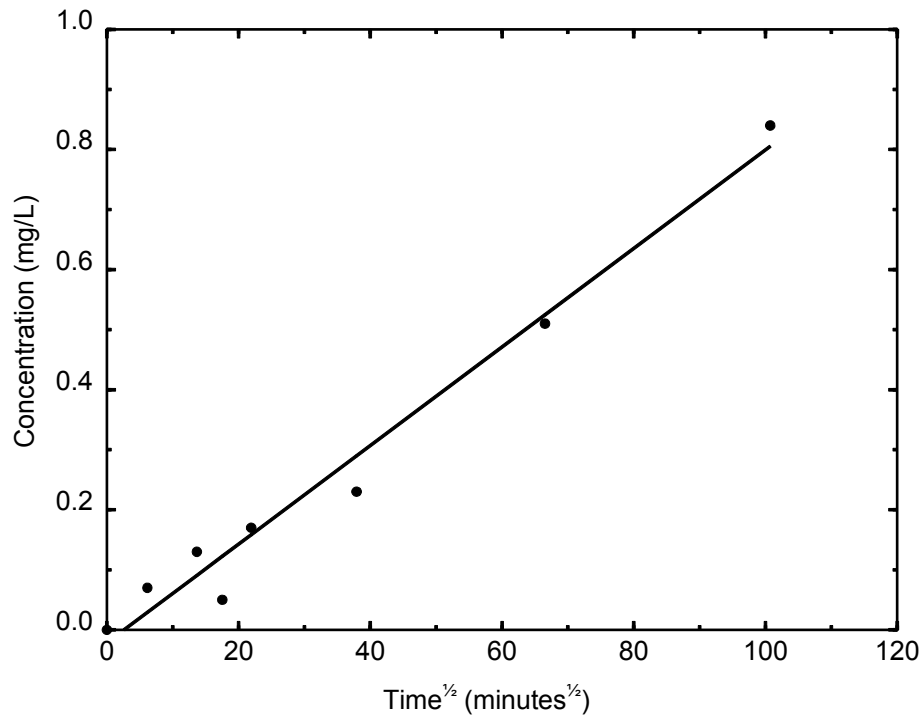


Figure 6. Br^- concentration vs. $\text{time}^{1/2}$ and regression line for Cell F, Core #3.

Table 2. Effective diffusivities and tortuosities of the three carbonate cores used in the diffusion experiments.

Core	Slope ($\text{mg/L}/\text{min}^{0.5}$)	r^2	D_p (Br^-) (cm^2/sec)	Tortuosity (τ)	D_p (^{14}C) (cm^2/sec)
1	3.97E-03	0.996	5.21E-06	.25	2.98E-06
2	3.93E-03	0.970	6.87E-06	.33	3.93E-06
3	8.21E-03	0.988	6.20E-06	.30	3.55E-06

Batch Experiments

Carbon-14 and ^{13}C results from the batch experiment are illustrated in Figures 7 and 8 along with a match of inverted Equation (50) to the data. Batch sorption experiment data are listed in Appendix 2. Recall that Equation (50) is the Laplace transform of combined Equation (45) and Equation (46) with the initial concentration for the kinetic sorption reaction set equal to

$$C_{\text{rapid}} = \frac{C_0}{\left(1 + \frac{\rho_b}{\phi} k_3\right)}. \text{ The data show an initial large loss of both } ^{14}\text{C} \text{ and } ^{13}\text{C} \text{ to the crushed}$$

limestone in the batch reactors. Carbon-14 decreased from 362 dpm/mL to 170 dpm/mL within the first 27 seconds while ^{13}C decreased from 3,383 per mil to 2,089 per mil within the first four minutes. As the experiment continued for the next 30 days, both ^{14}C activity and ^{13}C signature varied substantially from one time period to the next but with a general decreasing trend to

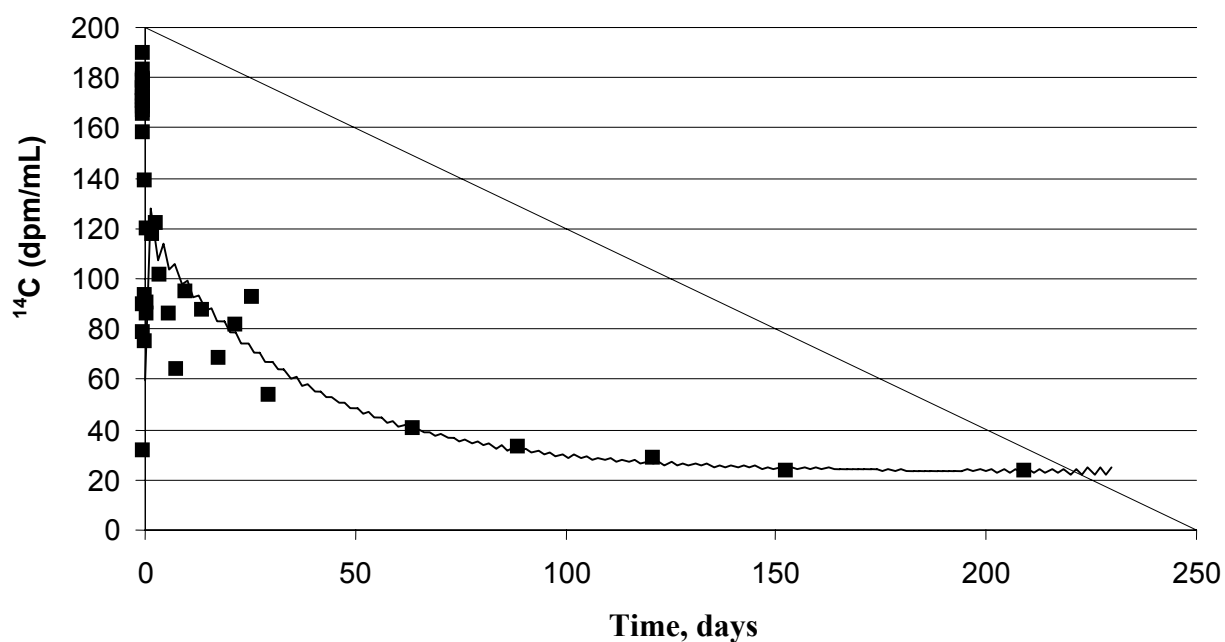


Figure 7. ^{14}C batch sorption data and fit of Equation (50) to the data. High-frequency oscillations in the fitted line are an artifact of the Laplace transform inversion algorithm.

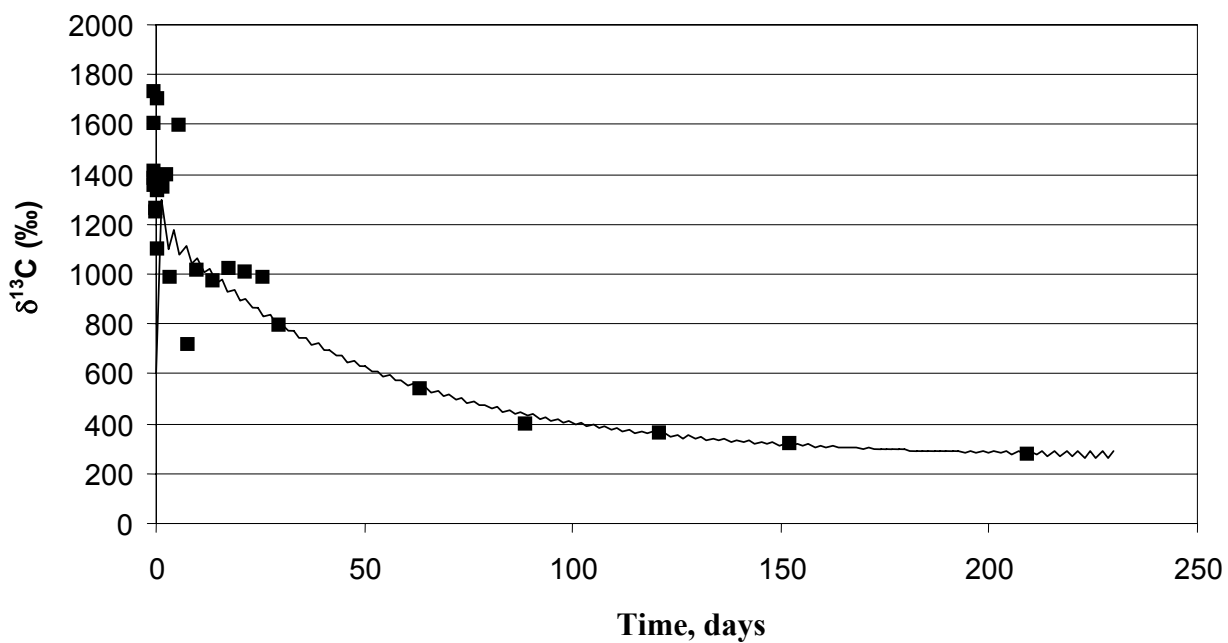


Figure 8. ^{13}C batch sorption data and fit of Equation (50) to the data. High-frequency oscillations in the fitted line are an artifact of the Laplace transform inversion algorithm.

53 dpm/mL and 784 per mil, respectively. By the end of the 210th day, ^{14}C activity had decreased to 23 dpm/mL and appears to be close to equilibrium. ^{13}C signature decreased from 3,833 per mil to 269 per mil but does not appear to have reached equilibrium. Mozeto *et al.* (1984a,b) showed similar results with ^{13}C batch experiments not reaching equilibrium up to one year. Control samples (batch reactors without any crushed carbonate material) showed little isotopic variation during the duration of the 210-day experiment.

The initial chemistry of Army #1 Water Well water utilized in the batch experiment and analyses of water in the batch reactors from different time periods are presented in Table 3. Also listed are carbonate mineral saturation indices (SI) and partial pressures of CO_2 (P_{CO_2}) for the batch waters calculated by the geochemical computer code WATEQF (Plummer *et al.*, 1976). Chemical analyses show a large decrease in concentrations of HCO_3^- , Ca^{2+} , and Mg^{2+} with a corresponding increase in pH in the batch reactors after the 45-day aging period. These variations along with the calculated P_{CO_2} and SI values indicate that carbonate minerals have precipitated on the freshly crushed limestone surfaces and that Army #1 Water Well water and the crushed limestone in the batch reactors have reached equilibrium prior to the start of the experiments. Analyses of batch reactor water for different time periods are similar to the batch reactor water chemistry prior to the start of the experiments (0 hour (no ^{14}C)). This indicates chemical stability during the experiments and suggests that the ^{14}C and ^{13}C loss observed during the experiments is not caused by dissolution or precipitation of carbonate minerals.

Table 3. Water chemistry of batch experiments.

Experiment	pH	HCO_3^- (mg/L)	Ca (mg/L)	Mg (mg/L)	LOG P_{CO_2}	SI calcite	SI dolomite
Army #1 Water Well	7.71	261	44.0	21.40	-2.27	0.41	0.84
0 hour blank*	8.43	120	9.7	7.20	-3.40	0.01	0.09
48 hour	8.17	130	12.8	8.52	-3.10	-0.09	-1.17
3 day	8.45	130	18.5	9.34	-3.40	0.33	0.55
10 day	8.58	124	14.7	8.13	-3.54	0.34	0.62
22 day	8.30	124	11.2	7.59	-3.25	-0.04	-0.05
26 day	8.61	116	9.6	7.55	-3.60	0.16	0.42
30 day	8.36	109	11.6	7.36	-3.37	-0.02	0.04
50 day	8.35	119	13.4	8.50	-3.32	0.06	0.13
120 day	8.36	106	12.2	6.28	-3.38	-0.01	-0.11
150 day	8.49	113	10.6	6.76	-3.49	0.08	0.17
210 day	8.51	112	9.9	5.34	-3.51	0.07	0.07

* no ^{13}C or ^{14}C added, 45 days of aging of water and crushed carbonate material

The values of k_1 , k_2 , and k_3 resulting in the solid curves shown in Figures 7 and 8 are listed in Table 4. The overall K_d values calculated from Equation (53) are also listed in Table 4. The equilibrium and rate constants obtained from the ^{14}C and ^{13}C data are in reasonably good agreement, with the constants tending to be slightly larger for ^{14}C . It should be noted that the curves shown in Figures 7 and 8 were not least squares fits to the ^{14}C and ^{13}C data sets, but rather they were obtained by manually adjusting the constants until a reasonable “eyeball” match to the

data was achieved. Initial estimates of k_3 were obtained using Equation (43) with C_{rapid} set equal to the average concentration of the samples measured over the first four hours of the tests. Least-squares fitting attempts proved less successful than manual “eyeball” fits because the large number of early-time data points and the scatter associated with these points resulted in poor k_1 and k_2 estimates. Least-squares fitting could probably have been improved by assigning high weights to the last five to six data points or by simply removing some of the early time data. However, these approaches were deemed to have as much subjectivity as the eyeball-fitting procedure, so the latter was used.

Table 4. Instantaneous distribution coefficient (k_3), forward and backward rate (k_1 and k_2), and the overall distribution coefficient (K_d) obtained from the batch experiments.

Isotope	k_3 (mL/g)	k_1 (1/day)	k_2 (g/mL-day)	K_d (mL/g)
^{14}C	4	0.022	0.0026	29.4
^{13}C	3.6	0.015	0.0021	23.6

Fracture Experiments

Details on the individual fracture experiments are outlined in Table 5. Analytical results of the fracture experiments are presented in Appendix 3.

Table 5. Br^- and ^{14}C fracture experiment parameters.

Experiment #	Tracer	Flow Rate (mL/min)	Pulse Length (sec)	C_0
2	Br^-	3.50	171	5.0 mg/L
3	Br^-	2.30	261	5.0 mg/L
4	Br^-	1.70	353	5.0 mg/L
5	Br^-	0.84	714	5.0 mg/L
6	^{14}C	0.82	732	295 dpm/mL
7	^{14}C	1.75	343	295 dpm/mL
8	^{14}C	2.35	255	320 dpm/mL
9	Br^- , ^{14}C	1.6 - 2.6	1,460	644 mg/L, 1,176 dpm/mL
10	Br^- , ^{14}C	2.7 - 3.2	3,244	589 mg/L, 943 dpm/mL

Br^- Tracer Experiments

Normalized Br^- concentrations as a function of volume eluted through the fracture are presented in Figure 9 for experiments 2 through 5. The same volume of tracer, 10 mL, was injected for each test but the injection rate and time of the experiment varied (Table 1). The breakthrough curves for the four experiments plot almost identically, indicating that (1) there was very little matrix diffusion in the system at the flow rates utilized, (2) the physical condition of the experimental apparatus was constant, and (3) the fracture configuration was unchanged throughout the experiments. If matrix diffusion was significant, a progressive broadening and flattening of breakthrough curve with decreasing flow rates would have been observed. Bromide mass recoveries for the four experiments were 92, 97, 90, and 93 percent, respectively.

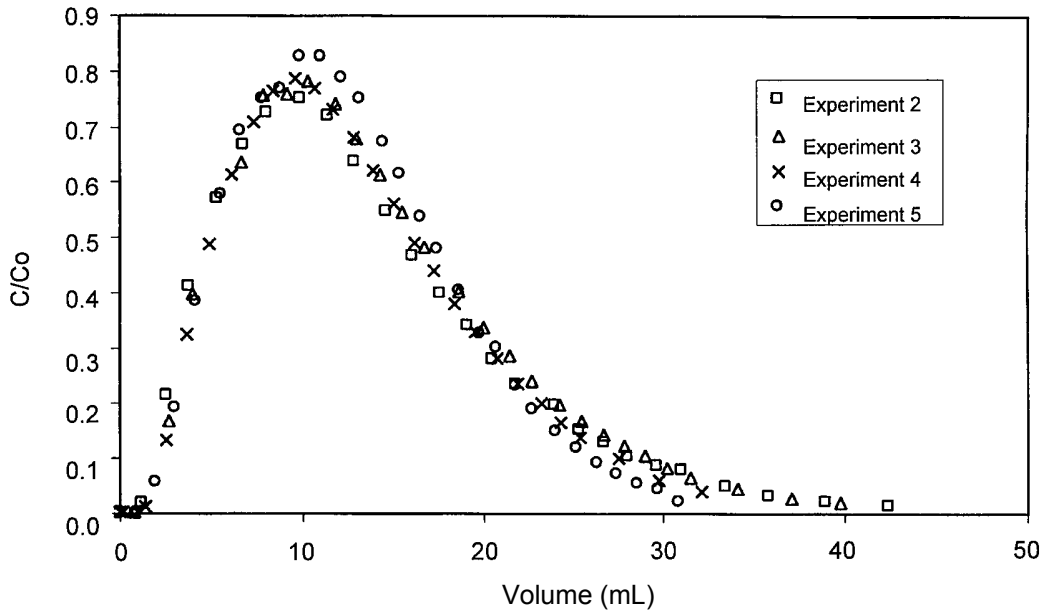


Figure 9. Br^- response as a function of volume in fracture experiments 2 through 5.

Not surprisingly, the best simultaneous RELAP fits to the four Br^- data sets (Figure 10) were obtained with a lumped matrix diffusion parameter of zero, indicating minimal matrix diffusion at the relatively high flow rates of the experiments. Table 6 provides the best-fitting model parameter values associated with the fits. Figure 10 shows that the RELAP fits are not great, which is taken as an indication that there is probably some preferential flow channeling through the fracture that results in tracer responses that are not well fit by the advection-dispersion equation (which assumes Fickian dispersion). Modeling studies by others (Moreno *et al.*, 1988; Moreno and Tsang, 1991; Thompson 1991) have shown that responses in highly channelized flow systems can deviate significantly from Fickian dispersion behavior. This interpretation is consistent with the observed partial filling of the fracture with calcite or dolomite crystals, and it is also supported by a relatively low best-fitting Peclet number of 1.75 (*i.e.*, much dispersion).

Because the high flow rates in the experiments would have tended to mask the effects of matrix diffusion, it was desirable to obtain an estimate of the maximum value of the lumped parameter $\frac{\phi}{b} \sqrt{D_m R_{ap}}$ that was still consistent with the Br^- data. To do this, the Br^- data from the lowest flow rate experiment, which should have had the greatest amount of matrix diffusion, was simulated using RELAP with successively larger values of the lumped matrix diffusion parameter. The results are shown in Figure 11. Figure 11 suggests that, over the range of flow rates used in the Br^- experiments, it was essentially impossible to distinguish between a lumped parameter of zero and a lumped parameter of about $0.0038 \text{ sec}^{-1/2}$. That is, only when the lumped parameter becomes significantly larger than $0.0038 \text{ sec}^{-1/2}$, does the RELAP simulation begin to deviate significantly from simulations having a lumped parameter of zero.

Table 6. RELAP model parameters providing the best simultaneous fits to the Br⁻ breakthrough curves (see Figure 11).

Flow Rate, mL/min	τ_f , min	Peclet No. = L_{Pe}/α_{Pe}	$\frac{\phi}{b}\sqrt{D_m}$, sec ^{-1/2}
3.5	2.10	1.75	0
2.3	3.20	1.75	0
1.7	4.32	1.75	0
0.84	8.75	1.75	0

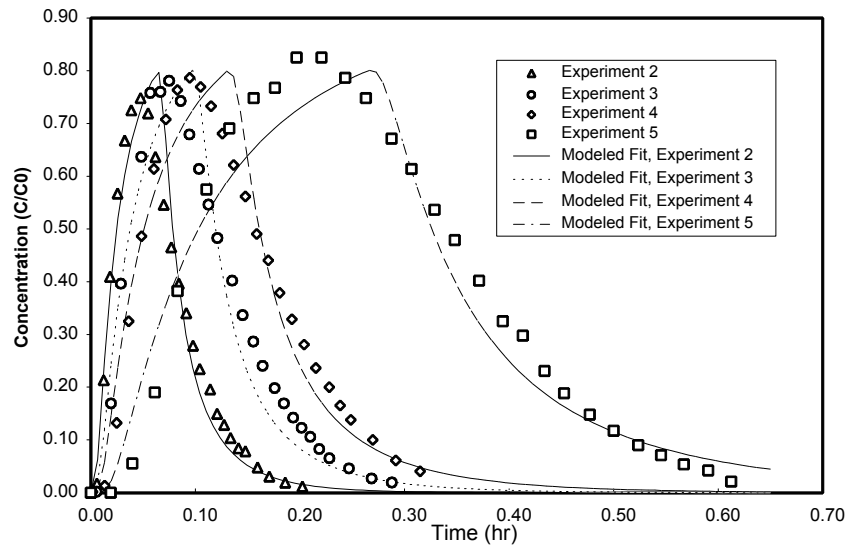


Figure 10. Br⁻ experimental data and RELAP modeled fits for fracture experiments 2 through 5.

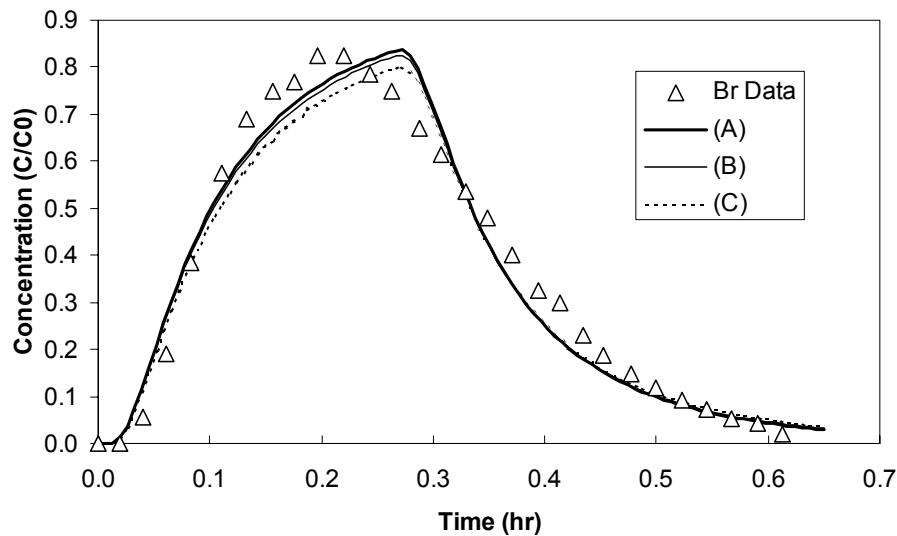


Figure 11. RELAP fits to the Br⁻ data for experiment 5 (0.84 mL/min): (A) $\frac{\phi}{b}\sqrt{D_m R_{ap}} = 0$,

(B) $\frac{\phi}{b}\sqrt{D_m R_{ap}} = 0.0012 \text{ sec}^{-1/2}$, and (C) $\frac{\phi}{b}\sqrt{D_m R_{ap}} = 0.0038 \text{ sec}^{-1/2}$.

An estimate of the maximum Br^- matrix diffusion coefficient consistent with the Br^- data sets can be obtained by substituting estimates of ϕ and b into $\frac{\phi}{b}\sqrt{D_m R_{ap}}$ and solving for D_m (with $R_{ap} = 1$ for Br^-) after this expression equal to the maximum fitted lumped parameter value ($0.0038 \text{ sec}^{-1/2}$). Using the matrix porosity obtained from mercury porosimetry measurements (0.066), and a fracture aperture estimate derived from $2b = Q\tau_f/L_fW$ (where b = fracture half aperture, Q = volumetric flow rate through fracture, τ_f = mean tracer residence time in the fracture, L_f = fracture length, and W = fracture width), the estimate of D_m for Br^- is approximately $4 \times 10^{-6} \text{ cm}^2/\text{sec}$. This value is in excellent agreement with the diffusion coefficients measured in the diffusion experiments (Table 3), even though the core used in the fracture experiments was not the same as the core used in the diffusion experiments.

^{14}C Tracer Experiments

Three ^{14}C tracer experiments were conducted in the fracture at approximately the same flow rates as the three lowest-flow-rate Br^- experiments. These experiments were conducted primarily to look at the groundwater chemistry exiting the fracture before and after each injection to determine whether conditions in the fracture were conducive to carbonate mineral precipitation. Precipitation of some of the ^{14}C would invalidate the assumption that all of the ^{14}C not exiting the fracture was being sorbed or exchanged within the core. ^{14}C breakthrough curves for these experiments are not shown, but the chemical data are provided in Table 7 along with the chemical data from the two multiple-tracer experiments discussed in the next section. The data in Table 7 indicate that there should have been little precipitation of ^{14}C in any of the fracture experiments since the water chemistry before and after each experiment changed little. However, water chemistry between each experiment did vary somewhat with time.

Table 7. Chemical data for ^{14}C fracture experiments.

Experiment	Time of Collection	pH	HCO_3^- (mg/L)	Ca (mg/L)	Mg (mg/L)	SI calcite	SI dolomite
6	Start	8.26	297	45.4	21.7	0.913	1.312
6	End	8.40	268	44.1	22.1	0.989	1.487
7	Start	8.29	273	45.2	21.7	0.907	1.302
7	End	8.32	268	45.2	21.9	0.927	1.347
8	Start	7.65	199	22.9	16.9	-0.101	-0.532
8	End	7.83	201	30.4	17.6	0.195	-0.045
9	Start	7.89	164	24.8	18.9	0.088	-0.142
9	End	8.19	165	24.1	19.6	0.366	0.445
10	Start	8.10	168	30.3	20.4	0.380	0.390
10	End	8.19	169	25.7	19.7	0.401	0.491

Simultaneous ^{14}C and Br^- Experiments

Breakthrough curves for experiments 9 and 10, in which ^{14}C and Br^- were injected into the fracture simultaneously, are presented in Figures 12 and 13 along with simultaneous RELAP fits to the data sets. The Br^- and ^{14}C data were fitted using the same mean residence time and Peclet number (since the tracers were injected simultaneously), but the diffusion coefficient for ^{14}C was assumed to be 0.57 times that of Br^- based on the ratio of the free water diffusion coefficients presented earlier. Also, the fracture and matrix retardation factors for Br^- were

assumed to be one (nonsorbing), while those for ^{14}C were adjusted to fit the ^{14}C data. Figures 12 and 13 show two fits to the ^{14}C data to illustrate the sensitivity of the ^{14}C fits to the matrix retardation factor. The lumped matrix diffusion parameter for Br^- was set equal to $0.0038 \text{ sec}^{-1/2}$,

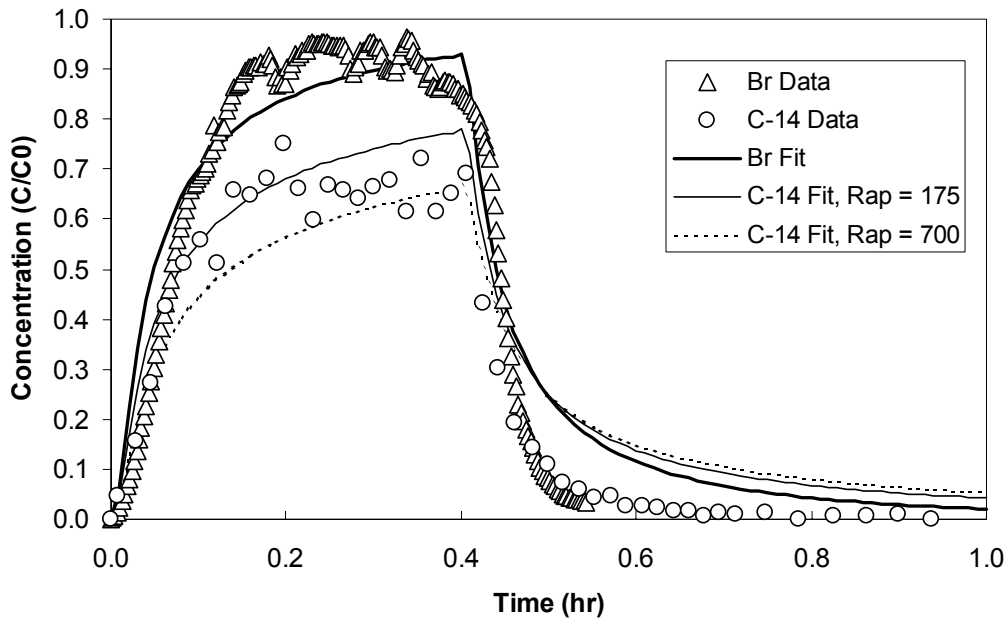


Figure 12. Br^- and ^{14}C data from experiment 9 and RELAP fits to the data.

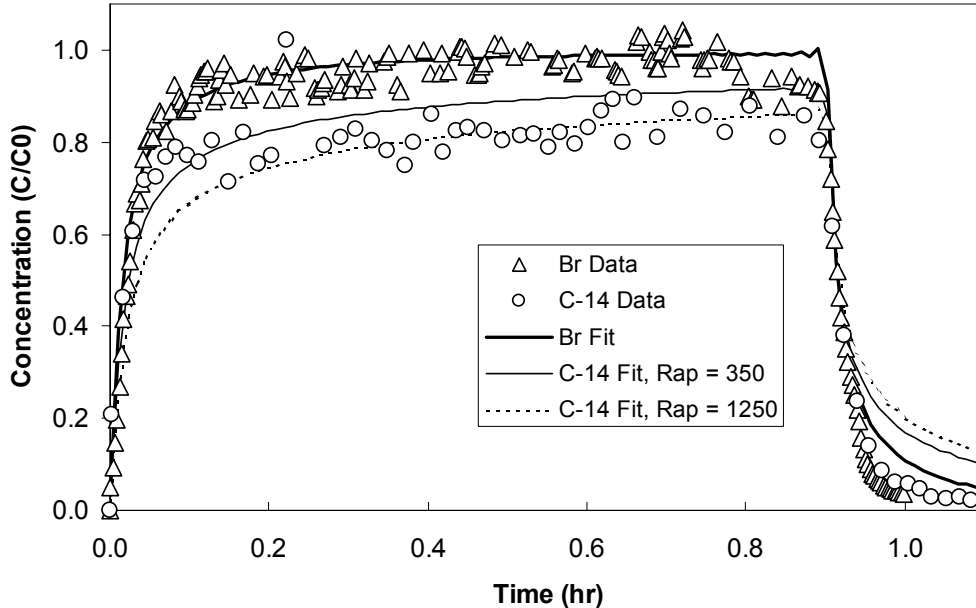


Figure 13. Br^- and ^{14}C data from experiment 10 and RELAP fits to the data.

the maximum value consistent with the Br^- data sets (Figure 11), as this value corresponds to a Br^- matrix diffusion coefficient that was in good agreement with the diffusion experiments (see above). Setting the lumped matrix diffusion parameter equal to its maximum value minimizes the fitted values of the ^{14}C retardation factors. Because of the short tracer residence times in the

experiments (no more than 10 minutes), it was assumed that only instantaneous sorption/exchange would affect the ^{14}C results. The forward sorption rate constants obtained for ^{14}C and ^{13}C in the batch sorption experiments (Table 5) indicate that less than 0.01 percent of the ^{14}C injected into the fracture should have sorbed kinetically.

The resulting best-fitting model parameters from RELAP for the Br^- and ^{14}C experiments are provided in Table 8. The parameters of greatest importance for this study are the fracture and matrix retardation factors for ^{14}C . The best-fitting ^{14}C fracture retardation factor, R_{af} , in both of the multiple tracer experiments was one. This value should not necessarily be taken to mean that there is no ^{14}C sorption or exchange occurring in the fractures, but rather it suggests that sorption/exchange occurs after a diffusive mass transfer step between the flowing water in the fractures and the surfaces onto which sorption/exchange occurs. The ranges of matrix retardation factors in Table 8 are quite large. The partition coefficients (K_d or k_3 values) associated with these retardation factors can be obtained from:

$$K_d = (R - 1) \frac{\phi}{\rho_b} \quad (54)$$

Substituting measured values of 0.066 for matrix porosity and 2.75 g/cm^3 for matrix bulk density into Equation (54) yields K_d estimates ranging from 4.2 mL/g ($R = 175$) to 30.0 mL/g ($R = 1250$) for the two fracture experiments.

Table 8. RELAP model parameters providing the best fits to the breakthrough curves in the two multiple tracer experiments (see Figures 12 and 13).¹

Parameter	Experiment 9	Experiment 10
Mean residence time (τ), min	6.3	2.6
Peclet No. = L_p/α_{pe}	0.75	0.5
$\text{Br}^- \frac{\phi}{b} \sqrt{D_m}$, $\text{sec}^{-1/2}$	0.0038	0.0038
$^{14}\text{C} \frac{\phi}{b} \sqrt{D_m}$, $\text{sec}^{-1/2}$	0.0029 ²	0.0029 ²
$^{14}\text{C} R_{\text{af}}$	1	1
$^{14}\text{C} R_{\text{ap}}$	175-700	350-1250

¹The Br^- and ^{14}C data from each experiment were fit simultaneously without considering the Br^- and ^{14}C data from the other experiment.

²The $\frac{\phi}{b} \sqrt{D_m}$ value for ^{14}C is $\sqrt{0.57}$ times that of Br^- .

Before comparing these values with the partition coefficients obtained from the batch experiments, it is necessary to account for differences in the specific surface areas of the materials used in the two types of experiments. The following relationship should “correct” partition coefficients measured in batch experiments so that they apply to the intact rock matrix used in the fracture experiments:

$$K_d^* = \frac{Z_p}{Z_b} K_d \quad (55)$$

where, K_d^* = corrected distribution coefficient, mL/g; K_d = distribution coefficient from batch experiments, mL/g; Z_p = specific surface area of matrix material, m^2/g ; and Z_b = specific surface area of crushed material, m^2/g .

Equation (55) applies to either k_3 , k_1/k_2 , or the overall K_d value obtained from the batch experiments. BET surface area measurements of both the crushed batch material and of the uncrushed carbonate aquifer matrix were conducted by Micromeretics Instrument Corp., yielding values of 2.4605 m^2/g and 1.5406 m^2/g , respectively. Substituting these values into Equation (55) yields a correction factor (Z_p/Z_b) of 1.54/2.46 = 0.626. The corrected values of k_3 and K_d from the batch experiments, and the range of k_3 values from the fracture experiments, are given in Table 9.

It is apparent from Table 9 that the k_3 values from the batch experiments are lower than in the fracture experiments. However, the values at the upper end of the range for the fractures are in relatively good agreement with the overall K_d values obtained after 210 days of sorption/exchange in the batch experiments. The tendency for the fracture experiments to yield higher k_3 values than the batch experiments could be caused by one or a combination of the following:

- The uncertainty in the matrix porosity of the core is significant, and the calculated K_d values are quite sensitive to matrix porosity. The matrix porosity of 0.066 used in Equation (54) was based on a single mercury porosimetry measurement on a piece of core that may not necessarily have been representative of the entire core, particularly near the fracture surfaces. If the actual matrix porosity near the fracture surfaces was half of that measured by mercury porosimetry, the range of K_d values from Equation (54) would be about a factor of two lower (see Table 1).
- Any fracture coating minerals present on the fracture surfaces (*e.g.*, calcite or dolomite) may have had a higher affinity for ^{14}C than the bulk matrix material that was tested in the batch experiments. Even if the affinity for ^{14}C was not higher, the sorption/exchange rates to these phases may have been high enough that they yielded a larger effective K_d value in the fracture experiments.
- If any ^{14}C was lost to the atmosphere caused by CO_2 gas evolution or isotopic exchange prior to entering or after exiting the fracture, the result would have been erroneously high retardation factors in the fracture experiments because the lost ^{14}C would have been attributed to sorption/exchange. Although careful measures were taken to avoid such losses, it is more likely that they would have occurred in the fracture experiments than in the more easily controlled batch experiments.

Table 9. Corrected distribution coefficients using Equation (55); overall distribution coefficients (K_d) from batch experiments; instantaneous distribution coefficients (k_3) values from fracture experiments.

Experiment	Isotope	k_3 (mL/g)	K_d (mL/g)
Batch	^{14}C	2.5	18.4
Batch	^{13}C	2.25	14.8
Column (low flow)	^{14}C	4.2 to 16.8	N/A
Column (high flow)	^{14}C	8.4 to 30.0	N/A

DISCUSSION

Implications for ^{14}C Transport at Large Scales and ^{14}C Groundwater Dating

According to Maloszewski and Zuber (1991), apparent ^{14}C groundwater ages can be corrected to true groundwater ages using the following formula:

$$\frac{t_a}{t_0} = R_{af} + (R_{ap} + R_{ak}) \frac{n_p^*}{n_f} \quad (56)$$

where, t_a = apparent ^{14}C groundwater age, yrs; t_0 = true groundwater age, yrs; $n_p^* = (1 - n_f)\phi$; and n_f = fracture porosity. Both fracture experiments in this study yielded $R_{af} = 1$. Using this result, Equation (56) can be written in terms of partition coefficients by substituting in the appropriate expressions for the retardation factors including $R_{ak} = \frac{(1 - \phi)\rho_d}{\phi} \frac{k_1}{k_2}$:

$$\frac{t_a}{t_0} = 1 + \left(1 + \frac{(1 - \phi)\rho_d}{\phi} k_3 + \frac{(1 - \phi)\rho_d}{\phi} \frac{k_1}{k_2} \right) \frac{n_p^*}{n_f} = 1 + \frac{n_p^*}{n_f} + \frac{(1 - \phi)\rho_d n_p^*}{\phi n_f} \left(k_3 + \frac{k_1}{k_2} \right) \quad (57)$$

We make one additional adjustment to this equation to account for the fact that the surface area per unit mass available for sorption in the matrix must decrease as the porosity decreases, which will cause the effective $(k_3 + k_1/k_2)$ value (mL/g) to also decrease (per Equation (55)). In the absence of specific surface area data as a function of porosity for carbonate rocks, we consider two end members for how surface area might vary as a function of porosity. One is that all pores have the same effective diameter and the number of pores is directly proportional to the porosity. In this case, the specific surface area will scale linearly with porosity. The other end member is that the number of pores remains the same, but the cross-sectional area of the pores varies linearly with porosity. In this case, the specific surface area will scale with the square root of porosity. These two cases do not necessarily cover the entire range of possibilities, but they are adopted here for convenience. We consider the most likely situation to be a combination of the two above end members, so we use a weighted linear combination of the two to correct the $(K_d = k_3 + k_1/k_2)$ values for specific surface area as a function of porosity:

$$Z_a = (1 - \sqrt{\phi}) \frac{\phi}{\phi_{\text{ref}}} + \sqrt{\phi} \sqrt{\frac{\phi}{\phi_{\text{ref}}}} \quad (58)$$

where, Z_a = correction factor for specific surface area as a function of matrix porosity,

ϕ_{ref} = reference porosity at which K_d values were measured.

The weight factors $(1 - \sqrt{\phi})$ and $\sqrt{\phi}$ are arbitrarily assigned so that as the matrix porosity approaches zero, the surface area becomes directly proportional to porosity (implying that all pores have the same diameter and it is the number of pores that varies), but as the porosity

increases, the surface area increases at a slower rate (implying an increasing percentage of larger pores). Introducing the correction factor, Z_a , to Equation (57):

$$\frac{t_a}{t_0} = 1 + \frac{n_p^*}{n_f} + \frac{(1 - \phi)\rho_d n_p^* Z_a}{\phi n_f} \left(k_3 + \frac{k_1}{k_2} \right) \quad (59)$$

and following the methodology of Maloszewski and Zuber (1991), Figure 14 shows graphically how t_a/t_0 varies as a function of n_p^*/n_f according to Equation (59). The lower curve shows the case for no sorption/exchange in the matrix, *i.e.*, all retardation is from the physical process of matrix diffusion. The upper and middle curves correspond to the largest and smallest values of ($K_d = k_3 + k_1/k_2$), respectively, determined in this study (2.5 and 30.0 mL/g - see Table 9). All curves correspond to a matrix porosity of 0.066, the measured porosity of the fractured core and the porosity to which all of the batch partition coefficients in Table 9 were “corrected.” This porosity was also used as the reference porosity for calculating Z_a for other matrix porosities. The curves in Figure 14 shift slightly upward as the matrix porosity decreases and slightly downward as it increases relative to the reference porosity. In going from a matrix porosity of 0.01 to 0.1 (a reasonable expected range for carbonate rocks at the NTS), the downward shift is about 26 percent or about 0.1 \log_{10} unit for a given value of n_p^*/n_f . However, for a given fracture porosity, the value of n_p^*/n_f also shifts (by almost 1 \log_{10} unit) as the matrix porosity increases, so the net effect of raising the matrix porosity from 0.01 to 0.1 is a significant increase in t_a/t_0 (by about a factor of 7.5).

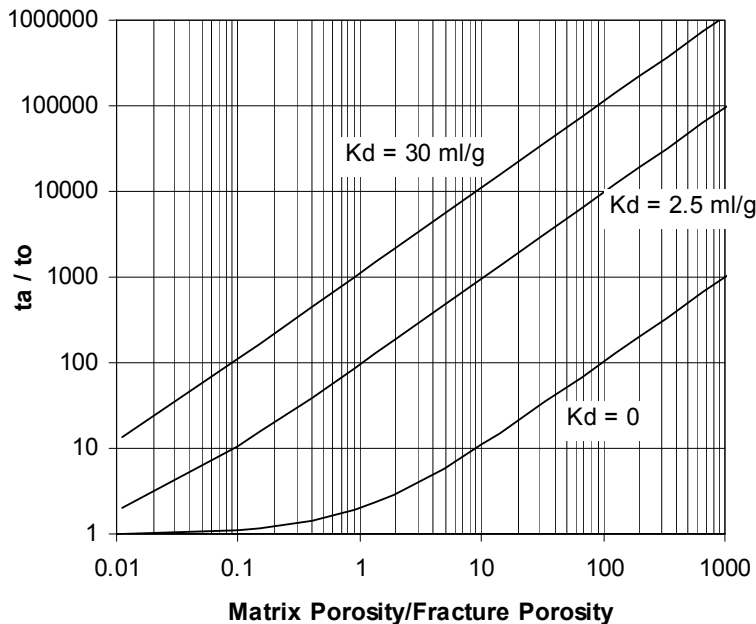


Figure 14. Ratio of apparent ^{14}C age to true groundwater age as a function of n_p^*/n_f for different ^{14}C K_d values. The upper two lines represent the lowest and highest K_d values from this study.

To put Figure 14 into practical perspective, Figure 15 is a plot of n_p^*/n_f as a function of fracture spacing assuming equally spaced, 1-mm-aperture fractures for three different matrix porosities ranging from 0.01 to 0.1. For a given fracture spacing and matrix porosity, a value of n_p^*/n_f can be read from the y-axis and used in Figure 14. The curves in Figure 15 can be easily shifted up or down to accommodate different fracture apertures. For instance, for 1-cm apertures, all curves would be shifted down by approximately one order of magnitude because the fracture porosity would increase by about an order of magnitude without significantly affecting n_p^* .

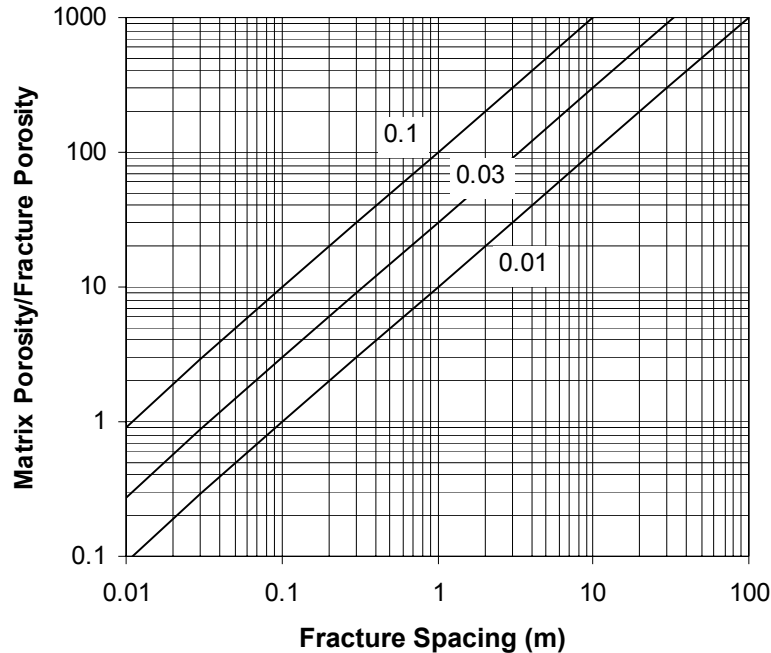


Figure 15. n_p^*/n_f for different fracture spacings and different matrix porosities (numbers on plot) assuming 1-mm aperture fractures.

Winograd and Thordarson (1975, pp. C17 and C19) reported matrix porosity values ranging from 0 to 0.09 for the LCA. The matrix porosities of the samples used in this study ranged from 0.015 to 0.066. Winograd and Thordarson (1975, pp. C15 and C18) also reported fracture apertures in cores from the LCA that ranged from 0.02 inches to 0.4 inches (0.05 to 1.0 cm). They reported a similar aperture range (<0.1 to 0.4 inches) for outcrops. These authors (1975, p. C18) also cited fracture porosity estimates for the LCA of 0 to 0.01, with an average of 0.001, as determined from the occurrence of partially filled fractures in cores. Fracture porosity estimates determined by geophysical logging were reported to range from 0 to 0.1 (Winograd and Thordarson, 1975, pp. C19), although these values are considered upper limits because of the limitation of geophysical logs to measure porosities in low porosity rocks. Kilroy (1992, pp. 56) determined porosity from specific storage and aquifer response to barometric fluctuations in one open fault and 11 wells that penetrated the carbonate-rock aquifers in eastern and southern Nevada. The estimates ranged from 0.01 to 0.044 with an average of 0.019.

If we use 0.01 and 0.1 as the lower and upper bounds for matrix porosity, and 0.0001 to 0.4 as the lower and upper bounds for fracture porosity in the LCA, then the effective bounds for

n_p^*/n_f become 0.25 to 1000. It is immediately apparent that the range of uncertainty for n_p^*/n_f (*i.e.*, over three orders of magnitude) is much greater than the range of uncertainty in the ^{14}C partition coefficient (about one order of magnitude, or the vertical distance between the two upper lines in Figure 14). Referring to Figure 14 and using the range of ^{14}C partition coefficients determined in this study, the ^{14}C age correction factors at the low end of the n_p^*/n_f range are 20 to 200, and at the high end of the range they are 100,000 to 1,000,000. The latter values suggest that even groundwater that is “dead” with respect to ^{14}C activity could have a very young “true” age if the matrix porosity is large relative to the fracture porosity. Because fracture spacings and apertures would be expected to vary from one location to another, the appropriate correction factor to apply may vary considerably for water samples collected from different locations. Samples taken from highly fractured units with large effective fracture porosities may have relatively small correction factors, while samples taken from units with only a few widely spaced fractures may have very large correction factors. One might expect that borehole samples may be biased toward the former because highly fractured units often contribute more flow to boreholes than less fractured units. Additional complications associated with estimating ^{14}C age correction factors include (1) not all visible fractures necessarily conduct water, (2) the matrix porosity may have considerable spatial variability, even at local scales, and (3) the matrix between fractures may not be entirely accessible by ^{14}C because of diffusion boundaries such as fractures filled with nonporous minerals. All of these factors will contribute to uncertainty in estimating true groundwater ages from ^{14}C ages.

The age correction factors discussed above can be applied to the apparent ^{14}C ages of groundwater collected from two wells along a proposed flowpath between Army #1 Water Well (23,000 years) and Amargosa Tracer Well #2 (32,000 years) assuming that there is no groundwater recharge or mixing of different groundwater masses along this flowpath. Using the smallest correction factor of approximately 20, the true groundwater ages become 1,150 years and 1,600 years, respectively, at the two wells. The linear distance between these wells is approximately 18,000 m, so the implied groundwater velocity is $18,000/(1,600-1,150) = 40$ m/yr. However, using a correction factor of 100,000 yields an implausible velocity of 200,000 m/yr, or about 23 m/hr. These velocities can be compared to velocity ranges of 1.8 to 18,000 m/yr calculated from the hydrologic data of Winograd and Thordarson (1975, p. C115) and 11 to 11,000 m/yr calculated from the data of Laczniaik *et al.* (1996, p. 20). Groundwater velocities calculated by Thomas *et al.* (1996, p. C61) for the Ash Meadows flow system using water chemistry and isotopic data and assuming an effective porosity of 0.02 were 26 to 43 m/yr. Clearly, the upper end of the range of ^{14}C correction factors estimated from this study yields groundwater velocities that appear to be at least an order of magnitude too high. However, the lower end of the range yields velocities that fall comfortably within the range of velocities estimated from hydrologic and water chemistry data. These comparisons suggest that either the effective value of n_p^*/n_f in the LCA is relatively small (perhaps because of limited diffusion distances into the matrix) or that the ^{14}C partition coefficients determined in this study overestimate effective partition coefficients at the field scale.

Recommendations for Future Experimental Studies to Support ^{14}C Groundwater Dating

Additional constraints on ^{14}C partition coefficients could be obtained by conducting crushed rock column transport studies in which ^{14}C and a conservative tracer (*e.g.*, Br^-) are

injected simultaneously at several different flow rates. Crushed rock column tests are much easier to conduct than fracture tests, and varying the flow rate would yield additional insights into sorption/exchange kinetics and into whether effective partition coefficients scale with time. Batch sorption/exchange studies using mineral phases identified on LCA fracture surfaces would yield information on how the presence of these phases might affect ^{14}C age correction factors. Desorption studies using ^{14}C and carbonate rocks would help place constraints on the reversibility of ^{14}C sorption/exchange processes.

The much greater range of uncertainty in n_p^*/n_f values compared to the range of uncertainty in ^{14}C partition coefficients (see “implications” section above) suggests that it would be a more effective use of resources to direct future studies at obtaining better estimates of n_p^*/n_f in the LCA than better estimates of ^{14}C partition coefficients. Long-term laboratory tracer experiments in fractured blocks of LCA material (preferably large blocks) would yield valuable information on effective solute diffusion distances into carbonate matrices as a function of time. These studies would not be conducted using ^{14}C as a tracer, but rather using conservative (nonsorbing) tracers. Such experiments would involve continuously injecting a tracer mix into a fractured block at a very low flow rate and measuring the effluent concentrations over time. The tracer responses over time would yield information on the effective distance that the tracers were able to diffuse into the matrix, or, more specifically, the effective matrix volume that participated in mass transfer with the fracture(s). This information could place some very useful constraints on values of n_p^*/n_f for estimating ^{14}C age correction factors.

Another valuable experimental exercise, albeit a more expensive one, would be to conduct field-scale tracer tests in the LCA using the stable isotope ^{13}C as a tracer along with one or more conservative tracers. To be effective in obtaining field-scale estimates of $^{14}\text{C}/^{13}\text{C}$ retardation factors, these tests would have to be cross-hole tests involving the injection of tracers into one well while pumping a nearby well. In addition to providing field-scale estimates of ^{14}C retardation factors, these tests would also provide estimates of fracture flow porosity in the LCA, which would help constrain estimates of n_p^*/n_f .

CONCLUSIONS

The ^{14}C and ^{13}C batch sorption experiments demonstrated that the sorption/exchange of carbon isotopes onto carbonate rocks involves both a very rapid process that can be assumed to be at equilibrium almost instantaneously and a relatively slow process. The instantaneous partition coefficient was about 4 mL/g, and the overall partition coefficient for the combined instantaneous and kinetic sorption processes was about 29 mL/g.

Fracture transport experiments demonstrated that, while ^{14}C was not delayed in its arrival time relative to a conservative solute tracer, it was significantly attenuated in normalized concentration relative to the conservative tracer. These results are consistent with significant sorption of the ^{14}C onto carbonate surfaces after a diffusive mass transfer step to the surfaces (*e.g.*, diffusion into the matrix followed by sorption). Partition coefficients deduced from the fracture experiments were not well constrained because of the high flow rates of the experiments, but the range of possible values was within a factor of two of the range of values from the batch sorption experiments. The Br^- matrix diffusion coefficients deduced from the fracture

experiments were in relatively good agreement with Br⁻ diffusion coefficients measured in separate diffusion experiments.

The partition coefficients determined for ¹⁴C in this study suggest that relatively large correction factors are necessary to correct apparent ¹⁴C groundwater ages to obtain “true” groundwater ages in the LCA. However, an examination of the factors contributing to the age correction factors indicates that the uncertainty in the correction factors is dominated by the uncertainty in the effective ratio of matrix porosity to fracture porosity rather than the uncertainty in the ¹⁴C partition coefficient. That being the case, it would appear to be a more effective use of resources to direct future investigations at obtaining better estimates of n_p^*/n_f in the LCA than better estimates of ¹⁴C partition coefficients.

REFERENCES

- Cameron, D.R. and A. Klute, 1977. Convective-dispersive solute transport with a combined equilibrium and kinetic adsorption model. *Water Resources Research*, 13(1):183-188.
- Garnier, J.M., 1985. Retardation of dissolved radiocarbon through a carbonated matrix. *Geochimica et Cosmochimica Acta*, 49:683-693.
- GeoTrans, Inc., 1995. A fracture/porous media model of tritium transport in underground weapons testing areas, Nevada Test Site. GeoTrans, Inc., Boulder, CO., DOE Contract No. AC08-92NV10972, 42 p.
- Gonfiantini, R., 1988. Carbon isotope exchange in karst groundwater. IAH 21st Congress: *Karst Hydrogeology and Karst Environmental Protection*, Guilin, China, pp. 832-837.
- Grisak, G.E. and J.F. Pickens, 1981. An analytical solution for solute transport through fractured media with matrix diffusion. *Journal of Hydrology*, 52:47-57.
- Grisak, G.E. and J.F. Pickens, 1980. Solute transport through fractured media, 1. The effect of matrix diffusion. *Water Resources Research*, 16(4):719-730.
- Grisak, G.E., J.F. Pickens and J.A. Cherry, 1980. Solute transport through fractured media, 2. Column study of fractured till. *Water Resources Research*, 16(4):731-739.
- Hurlbut, C.S., Jr. and C. Klein, 1977. Manual of Mineralogy, 19th. Ed. John Wiley & Sons, Inc., New York, 532 p.
- Kilroy, K.C., 1992. Aquifer storage characteristics of Paleozoic carbonate rocks in southeastern Nevada estimated from harmonic analysis of water-level fluctuations. University of Nevada, Reno, unpublished Ph.D. dissertation, 77 p.
- Klute, A., 1986. Methods of soil analysis: Part 1: Physical and mineralogic methods, 2nd ed., American Society of Agronomy, Madison.
- Laczniak, R.J., J.C. Cole, D.A. Sawyer and D.A. Trudeau, 1996. Summary of hydrogeologic controls on ground-water flow at the Nevada Test Site, Nye County, Nevada. U.S. Geological Survey Water-Resources Investigations Report 96-4109, 59 p.

- Maloszewski, P. and A. Zuber, 1991. Influence of matrix diffusion and exchange reactions on radiocarbon ages in fissured carbonate aquifers. *Water Resources Research*, 27(8):1937-1945.
- Maloszewski, P. and A. Zuber, 1990. Mathematical modeling of tracer behavior in short-term experiments in fissured rocks. *Water Resources Research*, 26(7):1517-1528.
- Maloszewski, P. and A. Zuber, 1985. On the theory of tracer experiments in fissured rocks with a porous matrix. *Journal of Hydrology*, 79:333-358.
- Moreno, L. and C. F. Tsang, 1991. Multiple-peak response to tracer injection tests in single fractures: A Numerical Study, *Water Resources Research*, 27(8): 2143-2150.
- Moreno, L., Y. W. Tsang, C. F. Tsang, F. V. Hale and I. Neretnieks, 1988. Flow and tracer transport in a single fracture: A stochastic model and its relation to some field observations, *Water Resources Research*, 24(12): 2033-2048.
- Mozeto, A.A., P. Fritz and R.M. Qureshi, 1984a. Laboratory study on carbon isotope uptake by calcite from carbonate in aqueous solution. Isotope Hydrology 1983, International Atomic Energy Agency, Vienna, 1984, p. 591-602.
- Mozeto, A.A., P. Fritz and E.J. Reardon, 1984b. Experimental observations on carbon isotope exchange in carbonate-water systems. *Geochimica et Cosmochimica Acta*, Vol. 48, p. 495-504.
- Mull, D.S., T.D. Liebermann, J.L. Smoot and L.H. Woosley Jr., 1988. Application of dye-tracing techniques for determining solute transport characteristics of ground water in karst terranes. U.S. Environmental Protection Agency, EPA 904/6-88-001, 103 pp.
- Neretnieks, I., 1981. Age dating of groundwater in fissured rock: Influence of water volume in micropores. *Water Resources Research*, 17(2):421-422.
- Neretnieks, I., 1980. Diffusion in the rock matrix. An important factor in radionuclide retardation? *Journal of Geophysical Research*, 85(B8):4379-4397.
- Neretnieks, I., T. Erikens and P. Tahtinen, 1982. Tracer movement in a single fissure in granitic rock: Some experimental results and their interpretation. *Water Resources Research*, 18(4):849-858.
- Parker, J.C. and M.Th. van Genuchten, 1984. Determining transport parameters from laboratory and field tracer experiments. Virginia Agricultural Experiment Station, Bull. 84-3, 51 pp.
- Plummer, L.N., B.F. Jones and A.H. Truesdell, 1976. WATEQF - A Fortran IV Version of WATEQ, A computer program for calculating chemical equilibrium of natural waters. U.S. Geological Survey Water-Resources Investigations Report 76-13, 70 p.
- Rasmuson, A. and I. Neretnieks, 1981. Migration of radionuclides in fissured rock: the influence of micropore diffusion and longitudinal dispersion. *Journal of Geophysical Research*, 86(B8):3749-3758.

- Reimus, P.W. and M.J. Haga, 1999. Analysis of tracer responses in the BULLION forced-gradient experiment at Pahute Mesa, Nevada. LA-13615-MS. Los Alamos National Laboratory, Los Alamos, New Mexico.
- Stumm, W. and J.J. Morgan, 1996. Aquatic Chemistry. John Wiley & Sons, Inc., New York, 1022 p.
- Sudicky, E.A. and E.O. Frind, 1982. Contaminant transport in fractured porous media: Analytical solutions for a system of parallel fractures. *Water Resources Research*, 18(6):1634-1642.
- Sudicky, E.A. and E.O. Frind, 1981. Carbon 14 dating of groundwater in confined aquifers: Implications of aquitard diffusion. *Water Resources Research*, 17(4):1060-1064.
- Tang, D.H., E.O. Frind and E.A. Sudicky, 1981. Contaminant transport in fractured porous media: Analytical solutions for a single fracture. *Water Resources Research*, 17(3):555-564.
- Thomas, J.M., A.H. Welch and M.D. Dettinger, 1996. Geochemistry and isotope hydrology of representative aquifers in the Great Basin region of Nevada, Utah, and adjacent states. U.S. Geological Survey Professional Paper 1409-C, 100 p.
- Thompson, M. E, 1991. Numerical simulation of solute transport in rough fractures, *J. Geophysical Res.*, 96(B3): 4157-4166.
- Vandergraff, T.T., D.M. Grondin and D.J. Drew, 1988. Laboratory radionuclide migration experiments. Materials Research Society, Symposium Proceedings, Vol. 112:159-168.
- Waddell, R.K., 1984. Solute-transport characteristics of fractured tuffs at Yucca Mountain, Nevada Test Site: A preliminary assessment. Geological Society of America Abstracts with Programs, Vol. 16(6):471.
- Winograd, I.J. and W. Thordarson, 1975. Hydrological and Hydrochemical framework, south-central Great Basin, Nevada-California, with special reference to the Nevada Test Site. U.S. Geological Survey Technical Letter NTS-117, 21 p.

APPENDIX A
LABORATORY RESULTS OF DIFFUSION EXPERIMENTS

	Sample #	Time (minutes)	Br ⁻ (mg/L)
Cell E / Core # 1	1-0 (Blank)	0	<0.01
	1-1	38	0.03
	1-2	104	0.04
	1-3	310	0.06
	1-4	478	0.07
	1-5	1,423	0.13
	1-6	4,441	0.28
	1-7	10,106	0.39
Cell B / Core # 2	2-0 (Blank)	0	<0.01
	2-1	35	0.03
	2-2	111	0.02
	2-3	308	0.02
	2-4	480	0.03
	2-5	1,385	0.10
	2-6	4,325	0.43
	2-7	10,085	0.46
	2-8	18,658	0.53
	2-9	26,079	0.61
	2-10	36,436	0.70
Cell F / Core # 3	3-0 (Blank)	0	<0.01
	3-1	38	0.07
	3-2	187	0.13
	3-3	307	0.05
	3-4	480	0.17
	3-5	1,438	0.23
	3-6	4,426	0.51
	3-7	10,147	0.84

APPENDIX B
LABORATORY RESULTS OF BATCH EXPERIMENTS

Experiment	Time (days)	$\delta^{13}\text{C}$ (‰)	^{14}C (dpm)
0 hour ¹	0.0000	3,383.4	362
27 second	0.0003	-	170
50 second	0.0006	-	189
1:07 minute	0.0008	-	179
1:20 minute	0.0009	-	182
1:34 minute	0.0011	-	171
1:48 minute	0.0013	-	178
2:03 minute	0.0014	-	175
2:19 minute	0.0016	-	165
2:38 minute	0.0018	-	175
2:52 minute	0.0020	-	166
3:07 minute	0.0022	-	173
3:22 minute	0.0023	-	170
4 minute	0.0026	2,089.0	157
1/4 hour	0.010	1,720.9	168
1/2 hour	0.021	1,347.3	178
1 hour	0.042	1,598.3	89
2 hour	0.083	1,373.3	31
4 hour	0.167	1,403.8	78
6 hour	0.250	1,351.8	74
8 hour	0.333	1,255.1	93
12 hour	0.500	1,239.5	138
16 hour	0.667	1,322.9	90
20 hour	0.833	1,095.7	85
24 hour	1.010	1,695.3	119
48 hour	2.087	1,341.5	117
3 day	3.038	1,388.6	121
4 day	4.010	982.2	101
6 day	6.007	1,590.6	85
8 day	8.024	708.9	63
10 day	10.08	1,010.6	94
14 day	14.06	962.2	87
18 day	17.97	1,016.1	68
22 day	22.00	996.7	81
26 day	25.96	980.1	92
30 day	29.98	784.2	53
60 day	64.07	532.4	40
90 day	88.99	393.6	32
120 day	121.20	355.8	28
150 day	152.83	311.1	23
210 day	209.76	268.8	23
Army #1 Water Well	-	-6.1	ND
0 hour blank ²	0.0000	-4.2	ND
24 hour blank ³	0.965	1,434.4	289
30 day blank ³	30.00	1,546.8	266
210 day blank ³	214.59	1,376.1	272

ND = non detect

¹45 days of aging of water and crushed carbonate material, then solid removed by filtration, then ^{13}C and ^{14}C added.

²No ^{13}C and ^{14}C added, 45 days of aging of water and crushed carbonate material.

³Army #1 Water Well water equilibrated with atmospheric CO_2 , then ^{13}C and ^{14}C added, no rock added.

APPENDIX C
LABORATORY RESULTS OF FRACTURE EXPERIMENTS

Fracture Experiment 2			
Time (Seconds)	Time (Hours)	Br ⁻ (mg/L)	Normalized Concentration
0	0.00	0.00	0.00
21	0.01	0.09	0.02
44	0.01	1.11	0.21
66	0.02	2.13	0.41
92	0.03	2.95	0.57
117	0.03	3.47	0.67
139	0.04	3.77	0.73
171	0.05	3.89	0.75
197	0.05	3.74	0.72
222	0.06	3.31	0.64
251	0.07	2.84	0.55
277	0.08	2.42	0.47
303	0.08	2.06	0.40
329	0.09	1.77	0.34
352	0.10	1.45	0.28
375	0.10	1.22	0.23
411	0.11	1.02	0.20
435	0.12	0.78	0.15
459	0.13	0.67	0.13
481	0.13	0.54	0.10
508	0.14	0.44	0.08
532	0.15	0.41	0.08
574	0.16	0.25	0.05
615	0.17	0.16	0.03
669	0.19	0.10	0.02
728	0.20	0.06	0.01

Fracture Experiment 3			
Time (Seconds)	Time (Hours)	Br ⁻ (mg/L)	Normalized Activity
0	0.00	0.00	0.00
20	0.01	0.01	0.00
70	0.02	0.88	0.17
104	0.03	2.06	0.40
174	0.05	3.31	0.64
205	0.06	3.94	0.76
240	0.07	3.95	0.76
270	0.08	4.06	0.78
310	0.09	3.86	0.74
340	0.09	3.53	0.68
373	0.10	3.19	0.61
405	0.11	2.84	0.55
436	0.12	2.51	0.48
487	0.14	2.09	0.40
523	0.15	1.75	0.34
560	0.16	1.49	0.29

592	0.16	1.25	0.24
633	0.18	1.03	0.20
665	0.18	0.88	0.17
697	0.19	0.74	0.14
726	0.20	0.64	0.12
756	0.21	0.55	0.11
787	0.22	0.43	0.08
822	0.23	0.34	0.07
889	0.25	0.24	0.05
967	0.27	0.14	0.03
1,037	0.29	0.10	0.02

Fracture Experiment 4

Time (Seconds)	Time (Hours)	Br ⁻ (mg/L)	Normalized Activity
0	0.00	0.01	0.00
6	0.00	0.01	0.00
48	0.01	0.07	0.01
89	0.02	0.69	0.13
130	0.04	1.69	0.33
174	0.05	2.53	0.49
217	0.06	3.19	0.61
258	0.07	3.68	0.71
298	0.08	3.97	0.76
341	0.09	4.09	0.79
378	0.11	4.00	0.77
414	0.12	3.81	0.73
453	0.13	3.54	0.68
492	0.14	3.23	0.62
532	0.15	2.92	0.56
571	0.16	2.55	0.49
611	0.17	2.29	0.44
650	0.18	1.97	0.38
692	0.19	1.71	0.33
734	0.20	1.46	0.28
775	0.22	1.23	0.24
821	0.23	1.04	0.20
859	0.24	0.86	0.17
895	0.25	0.72	0.14
971	0.27	0.52	0.10
1,050	0.29	0.32	0.06
1,134	0.32	0.21	0.04

Fracture Experiment 5

Time (Seconds)	Time (Hours)	Br ⁻ (mg/L)	Normalized Activity
0	0.00	0.00	0.00
68	0.02	0.00	0.00
143	0.04	0.29	0.06
220	0.06	0.99	0.19
299	0.08	1.99	0.38
398	0.11	2.99	0.58

477	0.13	3.59	0.69
561	0.16	3.89	0.75
634	0.18	3.99	0.77
708	0.20	4.29	0.83
794	0.22	4.29	0.83
876	0.24	4.09	0.79
947	0.26	3.89	0.75
1,035	0.29	3.49	0.67
1,104	0.31	3.19	0.61
1,183	0.33	2.79	0.54
1,253	0.35	2.49	0.48
1,337	0.37	2.09	0.40
1,418	0.39	1.69	0.33
1,487	0.41	1.55	0.30
1,562	0.43	1.20	0.23
1,630	0.45	0.98	0.19
1,718	0.48	0.77	0.15
1,800	0.50	0.61	0.12
1,885	0.52	0.47	0.09
1,963	0.55	0.37	0.07
2,042	0.57	0.28	0.05
2,126	0.59	0.22	0.04
2,205	0.61	0.11	0.02

Fracture Experiment 6

Time (Seconds)	Time (Hours)	¹⁴ C (dpm/mL)	Normalized Activity
0	0.00	0	0.00
17	0.00	3	0.01
100	0.03	2	0.01
188	0.05	21	0.07
278	0.08	75	0.26
364	0.10	120	0.41
486	0.14	164	0.56
573	0.16	189	0.64
663	0.18	209	0.71
756	0.21	223	0.76
846	0.24	220	0.74
942	0.26	220	0.74
1,030	0.29	205	0.69
1,124	0.31	173	0.59
1,216	0.34	156	0.53
1,308	0.36	131	0.44
1,401	0.39	113	0.38
1,494	0.42	93	0.32
1,586	0.44	80	0.27
1,685	0.47	65	0.22
1,826	0.51	48	0.16
1,930	0.54	39	0.13
2,026	0.56	33	0.11
2,127	0.59	26	0.09

2,225	0.62	20	0.07
2,322	0.65	17	0.06
2,423	0.67	14	0.05
2,516	0.70	11	0.04
2,618	0.73	11	0.04
2,717	0.75	8	0.03
2,814	0.78	11	0.04
2,951	0.82	8	0.03
3,049	0.85	9	0.03
3,155	0.88	6	0.02
3,257	0.90	6	0.02
3,359	0.93	6	0.02
3,460	0.96	6	0.02
3,555	0.99	5	0.02
3,666	1.02	3	0.01
3,762	1.05	5	0.02
3,863	1.07	5	0.02
3,967	1.10	6	0.02
4,069	1.13	3	0.01
4,164	1.16	3	0.01
4,259	1.18	3	0.01
4,354	1.21	5	0.02
4,478	1.24	5	0.02
4,580	1.27	5	0.02
4,680	1.30	5	0.02
4,778	1.33	3	0.01

Fracture Experiment 7

Time (Seconds)	Time (Hours)	¹⁴ C (dpm/mL)	Normalized Activity
0	0.00	2	0.00
31	0.01	3	0.01
77	0.02	9	0.03
126	0.04	56	0.19
175	0.05	74	0.25
228	0.06	90	0.31
281	0.08	122	0.41
332	0.09	191	0.65
381	0.11	168	0.57
443	0.12	120	0.41
493	0.14	110	0.37
542	0.15	98	0.33
597	0.17	77	0.26
644	0.18	98	0.33
694	0.19	53	0.18
744	0.21	77	0.26
799	0.22	41	0.14
849	0.24	32	0.11
899	0.25	30	0.10
948	0.26	21	0.07
998	0.28	18	0.06

1,056	0.29	17	0.06
1,108	0.31	14	0.05
1,162	0.32	9	0.03
1,215	0.34	8	0.03
1,265	0.35	12	0.04
1,315	0.37	6	0.02
1,368	0.38	3	0.01
1,416	0.39	5	0.02
1,491	0.41	5	0.02
1,545	0.43	3	0.01
1,598	0.44	3	0.01
1,654	0.46	2	0.01
1,707	0.47	0	0.00
1,861	0.52	0	0.00
1,913	0.53	0	0.00
1,965	0.55	0	0.00
2,055	0.57	2	0.01

Fracture Experiment 8

Time (Seconds)	Time (Hours)	¹⁴ C (dpm/mL)	Normalized Activity
0	0.00	0	0.00
46	0.01	72	0.23
96	0.03	158	0.49
125	0.03	205	0.64
153	0.04	227	0.71
198	0.06	248	0.77
227	0.06	263	0.82
265	0.07	230	0.72
309	0.09	191	0.60
359	0.10	161	0.50
387	0.11	120	0.38
415	0.12	108	0.34
450	0.13	95	0.30
485	0.13	71	0.22
517	0.14	60	0.19
547	0.15	54	0.17
577	0.16	54	0.17
623	0.17	33	0.10
652	0.18	18	0.06
682	0.19	23	0.07
711	0.20	12	0.04
744	0.21	15	0.05
777	0.22	23	0.07
832	0.23	14	0.04
866	0.24	8	0.02
901	0.25	5	0.01
932	0.26	9	0.03
962	0.27	9	0.03
999	0.28	8	0.02
1,032	0.29	3	0.01

1,077	0.30	5	0.01
1,109	0.31	0	0.00
1,138	0.32	5	0.01
1,177	0.33	0	0.00
1,209	0.34	6	0.02
1,252	0.35	11	0.03
1,282	0.36	8	0.02
1,316	0.37	5	0.01
1,344	0.37	2	0.00
1,393	0.39	0	0.00
1,426	0.40	0	0.00
1,460	0.41	3	0.01
1,490	0.41	2	0.00
1,530	0.43	0	0.00
1,564	0.43	2	0.00
1,602	0.45	11	0.03
1,654	0.46	0	0.00
1,685	0.47	0	0.00
1,715	0.48	0	0.00

Fracture Experiment 9

Time (Seconds)	Time (Hours)	¹⁴ C (dpm/mL)	Normalized Activity
0	0.00	5.58	0.00
25	0.01	55.80	0.05
101	0.03	185.28	0.16
163	0.05	320.47	0.27
228	0.06	499.11	0.42
300	0.08	600.47	0.51
366	0.10	654.75	0.56
435	0.12	600.17	0.51
504	0.14	772.65	0.66
576	0.16	761.52	0.65
645	0.18	802.57	0.68
708	0.20	883.02	0.75
770	0.21	777.46	0.66
830	0.23	703.32	0.60
893	0.25	786.78	0.67
958	0.27	771.74	0.66
1,018	0.28	755.20	0.64
1,082	0.30	782.72	0.67
1,146	0.32	797.01	0.68
1,215	0.34	721.22	0.61
1,277	0.35	848.14	0.72
1,341	0.37	724.38	0.62
1,401	0.39	766.18	0.65
1,463	0.41	814.00	0.69
1,530	0.43	507.99	0.43
1,592	0.44	353.55	0.30
1,661	0.46	226.78	0.19
1,732	0.48	166.18	0.14

1,799	0.50	127.23	0.11
1,860	0.52	85.73	0.07
1,929	0.54	68.74	0.06
1,989	0.55	51.44	0.04
2,058	0.57	54.15	0.05
2,120	0.59	32.80	0.03
2,184	0.61	32.80	0.03
2,249	0.62	27.53	0.02
2,313	0.64	21.37	0.02
2,374	0.66	19.71	0.02
2,438	0.68	7.68	0.01
2,497	0.69	14.90	0.01
2,566	0.71	11.29	0.01
2,693	0.75	14.00	0.01
2,831	0.79	1.52	0.00
2,971	0.83	9.04	0.01
3,105	0.86	9.19	0.01
3,239	0.90	11.74	0.01
3,375	0.94	1.37	0.00
3,641	1.01	3.77	0.00
3,773	1.05	0.02	0.00

Time (seconds)	Time (hours)	Br ⁻ (mg/L)	Normalized Concentration
0	0.00	0.97	0.00
6	0.00	2.37	0.00
16	0.00	4.65	0.01
26	0.01	8.98	0.01
36	0.01	15.61	0.02
46	0.01	23.50	0.04
56	0.02	31.25	0.05
66	0.02	41.73	0.06
76	0.02	52.03	0.08
86	0.02	62.56	0.10
96	0.03	74.40	0.12
106	0.03	87.60	0.14
116	0.03	103.40	0.16
126	0.04	118.60	0.18
136	0.04	132.30	0.21
146	0.04	145.80	0.23
156	0.04	161.90	0.25
166	0.05	178.50	0.28
176	0.05	195.40	0.30
186	0.05	211.60	0.33
196	0.05	229.10	0.36
206	0.06	246.30	0.38
216	0.06	263.80	0.41
226	0.06	278.50	0.43
236	0.07	295.10	0.46
246	0.07	308.10	0.48
256	0.07	328.80	0.51

266	0.07	344.70	0.54
276	0.08	360.00	0.56
286	0.08	374.60	0.58
296	0.08	385.60	0.60
306	0.09	396.90	0.62
316	0.09	411.50	0.64
326	0.09	423.60	0.66
336	0.09	429.80	0.67
346	0.10	431.30	0.67
356	0.10	439.10	0.68
366	0.10	442.30	0.69
376	0.10	447.20	0.69
386	0.11	452.00	0.70
396	0.11	458.60	0.71
406	0.11	470.40	0.73
416	0.12	475.50	0.74
426	0.12	507.50	0.79
436	0.12	485.90	0.75
446	0.12	498.40	0.77
456	0.13	505.60	0.79
466	0.13	505.60	0.79
476	0.13	526.20	0.82
486	0.14	537.70	0.83
496	0.14	545.50	0.85
506	0.14	555.50	0.86
516	0.14	557.50	0.87
526	0.15	559.50	0.87
536	0.15	563.60	0.88
546	0.15	573.80	0.89
556	0.15	578.00	0.90
566	0.16	582.20	0.90
576	0.16	582.20	0.90
586	0.16	584.30	0.91
596	0.17	584.30	0.91
606	0.17	582.20	0.90
616	0.17	588.60	0.91
626	0.17	586.40	0.91
636	0.18	586.40	0.91
646	0.18	597.10	0.93
656	0.18	592.80	0.92
666	0.19	584.30	0.91
676	0.19	569.70	0.88
686	0.19	557.50	0.87
696	0.19	569.70	0.88
706	0.20	561.60	0.87
716	0.20	561.50	0.87
726	0.20	582.20	0.90
736	0.20	578.00	0.90
746	0.21	586.40	0.91
756	0.21	599.30	0.93

766	0.21	595.00	0.92
776	0.22	599.30	0.93
786	0.22	603.70	0.94
796	0.22	603.60	0.94
806	0.22	603.60	0.94
816	0.23	612.40	0.95
826	0.23	614.60	0.95
836	0.23	612.40	0.95
846	0.24	612.40	0.95
856	0.24	612.40	0.95
866	0.24	614.60	0.95
876	0.24	614.70	0.95
886	0.25	614.60	0.95
896	0.25	612.40	0.95
906	0.25	610.20	0.95
916	0.25	610.20	0.95
926	0.26	610.20	0.95
936	0.26	608.00	0.94
946	0.26	610.20	0.95
956	0.27	610.20	0.95
966	0.27	605.80	0.94
976	0.27	597.10	0.93
986	0.27	580.10	0.90
996	0.28	573.80	0.89
1,006	0.28	582.20	0.90
1,016	0.28	586.40	0.91
1,026	0.29	603.60	0.94
1,036	0.29	603.60	0.94
1,046	0.29	603.60	0.94
1,056	0.29	612.40	0.95
1,066	0.30	614.70	0.95
1,076	0.30	614.70	0.95
1,086	0.30	608.00	0.94
1,096	0.30	608.00	0.94
1,106	0.31	608.00	0.94
1,116	0.31	597.10	0.93
1,126	0.31	582.20	0.90
1,136	0.32	578.00	0.90
1,146	0.32	580.10	0.90
1,156	0.32	578.00	0.90
1,166	0.32	575.90	0.89
1,176	0.33	584.30	0.91
1,186	0.33	597.10	0.93
1,196	0.33	608.00	0.94
1,206	0.34	612.40	0.95
1,216	0.34	621.30	0.96
1,226	0.34	619.10	0.96
1,236	0.34	616.90	0.96
1,246	0.35	603.60	0.94
1,256	0.35	595.00	0.92

1,275	0.35	586.40	0.91
1,285	0.36	584.30	0.91
1,295	0.36	567.70	0.88
1,305	0.36	573.80	0.89
1,315	0.37	575.90	0.89
1,325	0.37	557.50	0.87
1,335	0.37	555.50	0.86
1,345	0.37	553.50	0.86
1,355	0.38	555.50	0.86
1,365	0.38	563.60	0.88
1,375	0.38	565.60	0.88
1,385	0.38	563.60	0.88
1,395	0.39	563.60	0.88
1,405	0.39	559.50	0.87
1,415	0.39	553.50	0.86
1,425	0.40	553.50	0.86
1,435	0.40	545.50	0.85
1,445	0.40	547.50	0.85
1,455	0.40	543.60	0.84
1,465	0.41	539.60	0.84
1,475	0.41	537.70	0.83
1,485	0.41	531.90	0.83
1,495	0.42	526.10	0.82
1,505	0.42	522.40	0.81
1,515	0.42	511.20	0.79
1,525	0.42	500.20	0.78
1,535	0.43	487.70	0.76
1,545	0.43	478.90	0.74
1,555	0.43	465.30	0.72
1,565	0.43	434.40	0.67
1,575	0.44	404.10	0.63
1,585	0.44	373.30	0.58
1,595	0.44	342.20	0.53
1,605	0.45	310.40	0.48
1,615	0.45	282.50	0.44
1,625	0.45	259.00	0.40
1,635	0.45	234.10	0.36
1,645	0.46	209.30	0.33
1,655	0.46	185.10	0.29
1,665	0.46	171.50	0.27
1,675	0.47	148.50	0.23
1,685	0.47	136.10	0.21
1,695	0.47	125.20	0.19
1,705	0.47	115.70	0.18
1,715	0.48	106.40	0.17
1,725	0.48	99.80	0.15
1,735	0.48	92.80	0.14
1,745	0.48	83.90	0.13
1,755	0.49	73.90	0.11
1,765	0.49	66.56	0.10

1,775	0.49	61.00	0.09
1,785	0.50	56.59	0.09
1,795	0.50	53.36	0.08
1,805	0.50	49.48	0.08
1,815	0.50	45.51	0.07
1,825	0.51	42.19	0.07
1,835	0.51	38.82	0.06
1,845	0.51	35.74	0.06
1,855	0.52	32.99	0.05
1,865	0.52	31.02	0.05
1,875	0.52	29.40	0.05
1,885	0.52	28.34	0.04
1,895	0.53	27.24	0.04
1,905	0.53	26.48	0.04
1,915	0.53	25.91	0.04
1,925	0.53	25.54	0.04
1,935	0.54	24.35	0.04
1,945	0.54	23.16	0.04
1,955	0.54	21.61	0.03
1,965	0.55	20.55	0.03
1,975	0.55	19.83	0.03
1,985	0.55	19.46	0.03
1,995	0.55	19.18	0.03
2,005	0.56	18.92	0.03
2,015	0.56	18.50	0.03
2,025	0.56	18.17	0.03
2,035	0.57	17.60	0.03
2,045	0.57	16.84	0.03
2,055	0.57	16.43	0.03
2,065	0.57	15.62	0.02
2,075	0.58	15.68	0.02
2,085	0.58	15.62	0.02
2,095	0.58	15.90	0.02
2,105	0.58	16.02	0.02
2,115	0.59	16.18	0.03
2,125	0.59	15.85	0.02
2,135	0.59	15.44	0.02
2,145	0.60	14.58	0.02
2,155	0.60	13.80	0.02
2,165	0.60	13.57	0.02
2,175	0.60	13.37	0.02
2,185	0.61	13.36	0.02
2,195	0.61	13.27	0.02
2,205	0.61	12.61	0.02
2,215	0.62	11.90	0.02
2,225	0.62	11.60	0.02
2,235	0.62	11.56	0.02
2,245	0.62	11.61	0.02
2,255	0.63	11.65	0.02
2,265	0.63	11.60	0.02

2,275	0.63	11.36	0.02
2,285	0.63	11.19	0.02
2,295	0.64	10.56	0.02
2,305	0.64	10.34	0.02
2,315	0.64	10.37	0.02
2,325	0.65	10.38	0.02
2,335	0.65	10.49	0.02
2,345	0.65	10.42	0.02
2,355	0.65	10.15	0.02
2,365	0.66	9.79	0.02
2,375	0.66	9.51	0.01
2,385	0.66	9.18	0.01
2,395	0.67	9.17	0.01
2,405	0.67	8.98	0.01
2,415	0.67	8.69	0.01
2,425	0.67	8.66	0.01
2,435	0.68	8.75	0.01
2,445	0.68	8.70	0.01
2,455	0.68	8.76	0.01
2,465	0.68	8.67	0.01
2,475	0.69	8.60	0.01
2,485	0.69	8.44	0.01
2,495	0.69	8.35	0.01
2,505	0.70	8.23	0.01
2,515	0.70	8.12	0.01
2,525	0.70	7.97	0.01
2,535	0.70	7.88	0.01
2,545	0.71	7.72	0.01
2,555	0.71	7.47	0.01
2,565	0.71	7.33	0.01
2,575	0.72	7.17	0.01
2,585	0.72	7.05	0.01
2,595	0.72	6.95	0.01
2,605	0.72	6.90	0.01
2,615	0.73	6.88	0.01
2,625	0.73	6.85	0.01
2,635	0.73	6.93	0.01
2,645	0.73	6.87	0.01
2,655	0.74	6.80	0.01
2,665	0.74	6.75	0.01
2,675	0.74	6.70	0.01
2,685	0.75	6.66	0.01
2,695	0.75	6.58	0.01
2,705	0.75	6.53	0.01
2,715	0.75	6.41	0.01
2,725	0.76	6.35	0.01
2,735	0.76	6.28	0.01
2,745	0.76	6.21	0.01
2,755	0.77	6.10	0.01
2,765	0.77	6.02	0.01

2,775	0.77	5.90	0.01
2,785	0.77	5.80	0.01
2,795	0.78	5.80	0.01
2,805	0.78	5.73	0.01
2,815	0.78	5.70	0.01
2,825	0.78	5.66	0.01
2,835	0.79	5.58	0.01
2,845	0.79	5.50	0.01
2,855	0.79	5.53	0.01
2,865	0.80	5.57	0.01
2,875	0.80	5.61	0.01
2,885	0.80	5.61	0.01
2,895	0.80	5.53	0.01
2,905	0.81	5.46	0.01
2,915	0.81	5.32	0.01
2,925	0.81	5.24	0.01
2,935	0.82	5.13	0.01
2,945	0.82	4.93	0.01
2,955	0.82	4.77	0.01
2,965	0.82	4.70	0.01
2,975	0.83	4.76	0.01
2,985	0.83	4.75	0.01
2,995	0.83	4.72	0.01
3,005	0.83	4.63	0.01
3,015	0.84	4.53	0.01
3,025	0.84	4.47	0.01
3,035	0.84	4.52	0.01
3,045	0.85	4.60	0.01
3,055	0.85	4.64	0.01
3,065	0.85	4.55	0.01
3,075	0.85	4.36	0.01
3,085	0.86	4.24	0.01
3,095	0.86	4.39	0.01
3,105	0.86	4.46	0.01
3,115	0.87	4.26	0.01
3,125	0.87	4.10	0.01
3,135	0.87	4.22	0.01
3,145	0.87	4.26	0.01
3,155	0.88	4.21	0.01
3,165	0.88	4.07	0.01
3,175	0.88	4.02	0.01
3,185	0.88	4.17	0.01
3,195	0.89	4.03	0.01
3,205	0.89	3.90	0.01
3,215	0.89	3.85	0.01
3,225	0.90	3.99	0.01
3,235	0.90	4.03	0.01
3,245	0.90	3.91	0.01
3,255	0.90	3.84	0.01
3,265	0.91	3.78	0.01

3,275	0.91	3.72	0.01
3,285	0.91	3.84	0.01
3,295	0.92	3.90	0.01
3,305	0.92	3.85	0.01
3,315	0.92	3.76	0.01
3,325	0.92	3.68	0.01
3,335	0.93	3.64	0.01
3,345	0.93	3.61	0.01
3,355	0.93	3.59	0.01
3,365	0.93	3.56	0.01
3,375	0.94	3.55	0.01
3,385	0.94	3.53	0.01
3,395	0.94	3.50	0.01
3,405	0.95	3.46	0.01
3,415	0.95	3.41	0.01
3,425	0.95	3.40	0.01
3,435	0.95	3.44	0.01
3,445	0.96	3.48	0.01
3,455	0.96	3.57	0.01
3,465	0.96	3.62	0.01
3,475	0.97	3.65	0.01
3,485	0.97	3.63	0.01
3,495	0.97	3.62	0.01
3,505	0.97	3.58	0.01
3,515	0.98	3.63	0.01
3,525	0.98	3.69	0.01
3,535	0.98	3.62	0.01
3,545	0.98	3.60	0.01
3,555	0.99	3.58	0.01
3,565	0.99	3.94	0.01
3,575	0.99	3.94	0.01
3,585	1.00	3.97	0.01
3,595	1.00	3.95	0.01
3,605	1.00	3.98	0.01
3,615	1.00	3.76	0.01
3,625	1.01	3.60	0.01
3,635	1.01	3.56	0.01
3,645	1.01	3.55	0.01
3,655	1.02	3.51	0.01
3,665	1.02	3.48	0.01
3,675	1.02	3.48	0.01
3,685	1.02	3.50	0.01
3,695	1.03	3.58	0.01
3,705	1.03	3.69	0.01
3,715	1.03	3.73	0.01
3,725	1.03	3.86	0.01
3,735	1.04	3.84	0.01
3,745	1.04	3.85	0.01
3,755	1.04	3.84	0.01
3,765	1.05	3.83	0.01

3,775	1.05	3.81	0.01
3,785	1.05	3.74	0.01
3,795	1.05	3.60	0.01
3,805	1.06	3.51	0.01
3,815	1.06	3.38	0.01
3,825	1.06	3.31	0.01
3,835	1.07	3.48	0.01
3,845	1.07	3.68	0.01
3,855	1.07	3.71	0.01
3,865	1.07	3.57	0.01
3,875	1.08	3.47	0.01
3,885	1.08	3.26	0.01
3,895	1.08	3.27	0.01
3,905	1.08	3.56	0.01
3,915	1.09	3.64	0.01
3,925	1.09	3.44	0.01
3,935	1.09	3.25	0.01
3,945	1.10	3.19	0.00
3,955	1.10	3.23	0.01
3,965	1.10	3.31	0.01
3,975	1.10	3.48	0.01
3,985	1.11	3.56	0.01
3,995	1.11	3.52	0.01
4,005	1.11	3.30	0.01
4,015	1.12	3.15	0.00
4,025	1.12	3.18	0.00
4,035	1.12	3.25	0.01
4,045	1.12	3.35	0.01
4,055	1.13	3.47	0.01
4,065	1.13	3.40	0.01
4,075	1.13	3.27	0.01
4,085	1.13	3.24	0.01
4,095	1.14	3.09	0.00
4,105	1.14	3.06	0.00
4,115	1.14	3.16	0.00
4,125	1.15	3.30	0.01
4,135	1.15	3.41	0.01
4,145	1.15	3.40	0.01
4,155	1.15	3.27	0.01
4,165	1.16	3.08	0.00
4,175	1.16	3.02	0.00
4,185	1.16	2.97	0.00
4,195	1.17	3.03	0.00
4,205	1.17	3.24	0.01
4,215	1.17	3.30	0.01
4,225	1.17	3.30	0.01
4,235	1.18	3.16	0.00
4,245	1.18	3.00	0.00
4,255	1.18	2.95	0.00
4,265	1.18	2.97	0.00

4,275	1.19	3.13	0.00
4,285	1.19	3.30	0.01
4,295	1.19	3.31	0.01
4,305	1.20	3.30	0.01
4,315	1.20	3.29	0.01
4,325	1.20	3.30	0.01
4,335	1.20	3.26	0.01
4,345	1.21	3.24	0.01
4,355	1.21	3.22	0.00
4,365	1.21	3.21	0.00
4,375	1.22	3.07	0.00
4,385	1.22	2.91	0.00
4,395	1.22	2.91	0.00
4,405	1.22	3.06	0.00
4,415	1.23	2.94	0.00
4,425	1.23	2.90	0.00
4,435	1.23	2.88	0.00
4,445	1.23	2.84	0.00
4,455	1.24	2.83	0.00
4,465	1.24	2.86	0.00
4,475	1.24	2.84	0.00
4,485	1.25	2.82	0.00
4,495	1.25	2.82	0.00
4,505	1.25	2.85	0.00
4,515	1.25	2.85	0.00
4,525	1.26	2.97	0.00
4,535	1.26	2.84	0.00
4,545	1.26	2.91	0.00
4,555	1.27	2.99	0.00
4,565	1.27	3.08	0.00
4,575	1.27	3.13	0.00
4,585	1.27	3.07	0.00
4,595	1.28	3.04	0.00
4,605	1.28	3.06	0.00
4,615	1.28	3.04	0.00
4,625	1.28	3.04	0.00
4,635	1.29	2.92	0.00
4,645	1.29	2.94	0.00
4,655	1.29	2.94	0.00
4,665	1.30	2.99	0.00
4,675	1.30	2.99	0.00
4,685	1.30	2.99	0.00
4,695	1.30	2.96	0.00
4,705	1.31	2.89	0.00
4,715	1.31	2.82	0.00
4,725	1.31	2.86	0.00
4,735	1.32	2.79	0.00
4,745	1.32	2.74	0.00
4,755	1.32	2.75	0.00
4,765	1.32	2.79	0.00

4,775	1.33	2.80	0.00
4,785	1.33	2.81	0.00
4,795	1.33	2.80	0.00
4,805	1.33	2.91	0.00
4,815	1.34	2.86	0.00
4,825	1.34	2.90	0.00
4,835	1.34	2.91	0.00
4,845	1.35	2.81	0.00
4,855	1.35	2.78	0.00
4,865	1.35	2.78	0.00
4,875	1.35	2.76	0.00
4,885	1.36	2.74	0.00
4,895	1.36	2.78	0.00
4,905	1.36	2.84	0.00
4,915	1.37	2.81	0.00
4,925	1.37	2.76	0.00
4,935	1.37	2.77	0.00
4,945	1.37	2.75	0.00
4,955	1.38	2.75	0.00
4,965	1.38	2.76	0.00
4,975	1.38	2.79	0.00
4,985	1.38	2.88	0.00
4,995	1.39	2.95	0.00
5,005	1.39	3.07	0.00
5,015	1.39	3.13	0.00
5,025	1.40	3.20	0.00
5,035	1.40	3.25	0.01
5,045	1.40	3.28	0.01
5,055	1.40	3.30	0.01
5,065	1.41	3.26	0.01

Fracture Experiment 10			
Time (Seconds)	Time (Hours)	¹⁴ C (dpm/mL)	Normalized Activity
0	0.00	0	0.00
8	0.00	197	0.21
58	0.02	437	0.46
107	0.03	571	0.61
157	0.04	674	0.72
206	0.06	684	0.73
255	0.07	723	0.77
302	0.08	743	0.79
351	0.10	727	0.77
403	0.11	714	0.76
466	0.13	756	0.80
537	0.15	671	0.71
604	0.17	774	0.82
673	0.19	708	0.75
734	0.20	728	0.77
800	0.22	961	1.02

971	0.27	746	0.79
1,046	0.29	763	0.81
1,117	0.31	779	0.83
1,185	0.33	758	0.80
1,257	0.35	737	0.78
1,334	0.37	706	0.75
1,374	0.38	752	0.80
1,457	0.40	809	0.86
1,511	0.42	732	0.78
1,568	0.44	777	0.82
1,623	0.45	785	0.83
1,693	0.47	778	0.83
1,775	0.49	757	0.80
1,857	0.52	767	0.81
1,923	0.53	770	0.82
1,987	0.55	744	0.79
2,043	0.57	773	0.82
2,105	0.58	750	0.80
2,166	0.60	784	0.83
2,223	0.62	819	0.87
2,280	0.63	839	0.89
2,327	0.65	755	0.80
2,378	0.66	845	0.90
2,477	0.69	763	0.81
2,583	0.72	821	0.87
2,688	0.75	808	0.86
2,790	0.78	773	0.82
2,901	0.81	829	0.88
3,023	0.84	763	0.81
3,148	0.87	808	0.86
3,210	0.89	756	0.80
3,272	0.91	582	0.62
3,327	0.92	357	0.38
3,382	0.94	223	0.24
3,436	0.95	133	0.14
3,496	0.97	83	0.09
3,554	0.99	58	0.06
3,619	1.01	54	0.06
3,670	1.02	45	0.05
3,722	1.03	28	0.03
3,788	1.05	23	0.02
3,848	1.07	27	0.03
3,901	1.08	19	0.02
3,953	1.10	22	0.02
4,003	1.11	23	0.02
4,057	1.13	17	0.02
4,163	1.16	7	0.01
4,343	1.21	15	0.02
4,462	1.24	10	0.01
4,573	1.27	3	0.00

Time (seconds)	Time (hours)	Br ⁻ (mg/L)	Normalized Concentration
0	0.00	0	0.00
3	0.00	28.6	0.05
13	0.00	55.7	0.09
23	0.01	86.7	0.15
33	0.01	116.9	0.20
43	0.01	157.8	0.27
53	0.01	201	0.34
63	0.02	245.5	0.42
73	0.02	275.1	0.47
83	0.02	288.2	0.49
93	0.03	318.4	0.54
103	0.03	358.2	0.61
113	0.03	391.6	0.66
123	0.03	404.3	0.69
133	0.04	397.2	0.67
143	0.04	417.5	0.71
153	0.04	449.9	0.76
163	0.05	473	0.80
173	0.05	474.6	0.81
183	0.05	454.8	0.77
193	0.05	476.3	0.81
203	0.06	497.2	0.84
213	0.06	513.4	0.87
223	0.06	511.6	0.87
233	0.06	506.1	0.86
243	0.07	491.9	0.84
253	0.07	484.9	0.82
263	0.07	504.3	0.86
273	0.08	509.7	0.87
283	0.08	526.4	0.89
293	0.08	543.5	0.92
303	0.08	537.7	0.91
313	0.09	530.1	0.90
323	0.09	522.6	0.89
333	0.09	513.4	0.87
343	0.10	511.6	0.87
353	0.10	513.4	0.87
363	0.10	520.8	0.88
373	0.10	520.7	0.88
383	0.11	532	0.90
393	0.11	541.6	0.92
403	0.11	553.3	0.94
413	0.11	557.2	0.95
423	0.12	561.2	0.95
433	0.12	561.2	0.95
443	0.12	565.2	0.96
453	0.13	563.2	0.96
463	0.13	549.4	0.93

473	0.13	522.6	0.89
483	0.13	530.1	0.90
493	0.14	551.3	0.94
503	0.14	563.2	0.96
513	0.14	571.3	0.97
523	0.15	543.5	0.92
533	0.15	530.1	0.90
543	0.15	557.2	0.95
553	0.15	569.3	0.97
563	0.16	555.2	0.94
573	0.16	522.6	0.89
583	0.16	526.3	0.89
593	0.16	541.6	0.92
603	0.17	567.2	0.96
613	0.17	551.3	0.94
623	0.17	524.5	0.89
633	0.18	532	0.90
643	0.18	551.3	0.94
653	0.18	559.2	0.95
663	0.18	569.3	0.97
673	0.19	571.3	0.97
683	0.19	565.2	0.96
693	0.19	555.2	0.94
703	0.20	559.2	0.95
713	0.20	557.2	0.95
723	0.20	547.4	0.93
733	0.20	524.5	0.89
743	0.21	524.5	0.89
753	0.21	528.2	0.90
763	0.21	539.7	0.92
773	0.21	555.2	0.94
783	0.22	573.3	0.97
793	0.22	567.2	0.96
803	0.22	549.3	0.93
813	0.23	528.2	0.90
823	0.23	532	0.90
833	0.23	537.7	0.91
843	0.23	559.2	0.95
853	0.24	559.2	0.95
863	0.24	563.2	0.96
873	0.24	577.4	0.98
883	0.25	581.6	0.99
893	0.25	577.4	0.98
903	0.25	567.2	0.96
913	0.25	547.4	0.93
923	0.26	539.7	0.92
933	0.26	530.1	0.90
943	0.26	537.7	0.91
953	0.26	539.6	0.92
963	0.27	547.4	0.93

973	0.27	551.3	0.94
983	0.27	565.2	0.96
993	0.28	571.3	0.97
1,003	0.28	581.6	0.99
1,013	0.28	577.4	0.98
1,023	0.28	557.2	0.95
1,033	0.29	535.8	0.91
1,043	0.29	545.4	0.93
1,053	0.29	567.2	0.96
1,063	0.30	583.7	0.99
1,073	0.30	567.2	0.96
1,083	0.30	543.5	0.92
1,093	0.30	537.7	0.91
1,103	0.31	553.3	0.94
1,113	0.31	577.5	0.98
1,123	0.31	583.7	0.99
1,133	0.31	555.2	0.94
1,143	0.32	541.6	0.92
1,153	0.32	537.7	0.91
1,163	0.32	549.3	0.93
1,173	0.33	571.3	0.97
1,183	0.33	579.5	0.98
1,193	0.33	581.6	0.99
1,203	0.33	565.2	0.96
1,213	0.34	553.3	0.94
1,223	0.34	533.9	0.91
1,233	0.34	547.4	0.93
1,243	0.35	573.3	0.97
1,253	0.35	579.5	0.98
1,263	0.35	583.7	0.99
1,273	0.35	579.5	0.98
1,283	0.36	579.5	0.98
1,293	0.36	565.2	0.96
1,303	0.36	545.4	0.93
1,313	0.36	535.8	0.91
1,323	0.37	539.7	0.92
1,333	0.37	547.4	0.93
1,343	0.37	563.2	0.96
1,353	0.38	583.7	0.99
1,363	0.38	573.3	0.97
1,373	0.38	545.5	0.93
1,383	0.38	541.6	0.92
1,393	0.39	553.3	0.94
1,403	0.39	569.3	0.97
1,413	0.39	585.7	0.99
1,423	0.40	587.8	1.00
1,433	0.40	577.4	0.98
1,443	0.40	575.4	0.98
1,453	0.40	559.2	0.95
1,463	0.41	547.4	0.93

1,473	0.41	541.6	0.92
1,483	0.41	549.3	0.93
1,493	0.41	559.2	0.95
1,503	0.42	583.7	0.99
1,513	0.42	592.1	1.01
1,523	0.42	581.6	0.99
1,533	0.43	561.2	0.95
1,543	0.43	543.5	0.92
1,553	0.43	555.3	0.94
1,563	0.43	573.3	0.97
1,573	0.44	585.7	0.99
1,583	0.44	592.1	1.01
1,593	0.44	592.1	1.01
1,603	0.45	589.9	1.00
1,613	0.45	579.5	0.98
1,623	0.45	553.3	0.94
1,633	0.45	541.6	0.92
1,643	0.46	547.4	0.93
1,653	0.46	557.2	0.95
1,663	0.46	557.2	0.95
1,673	0.46	559.2	0.95
1,683	0.47	567.2	0.96
1,693	0.47	571.3	0.97
1,703	0.47	577.5	0.98
1,713	0.48	583.7	0.99
1,723	0.48	589.9	1.00
1,733	0.48	589.9	1.00
1,743	0.48	596.3	1.01
1,753	0.49	592.1	1.01
1,763	0.49	594.2	1.01
1,773	0.49	594.2	1.01
1,783	0.50	592	1.01
1,793	0.50	592.1	1.01
1,803	0.50	589.9	1.00
1,813	0.50	583.7	0.99
1,823	0.51	581.6	0.99
1,833	0.51	579.5	0.98
1,843	0.51	585.8	0.99
1,853	0.51	589.9	1.00
1,863	0.52	585.7	0.99
1,873	0.52	581.6	0.99
1,883	0.52	583.7	0.99
1,893	0.53	587.8	1.00
1,903	0.53	585.7	0.99
1,913	0.53	585.8	0.99
1,923	0.53	579.5	0.98
1,933	0.54	579.5	0.98
1,943	0.54	577.4	0.98
1,953	0.54	573.4	0.97
1,963	0.55	567.3	0.96

1,973	0.55	567.2	0.96
1,983	0.55	571.3	0.97
1,993	0.55	571.3	0.97
2,003	0.56	567.2	0.96
2,013	0.56	569.3	0.97
2,023	0.56	577.4	0.98
2,033	0.56	575.4	0.98
2,043	0.57	567.2	0.96
2,053	0.57	559.2	0.95
2,063	0.57	557.2	0.95
2,073	0.58	555.2	0.94
2,083	0.58	559.2	0.95
2,093	0.58	559.2	0.95
2,103	0.58	561.2	0.95
2,113	0.59	559.2	0.95
2,123	0.59	559.2	0.95
2,133	0.59	571.3	0.97
2,143	0.60	579.5	0.98
2,153	0.60	583.7	0.99
2,163	0.60	585.7	0.99
2,173	0.60	577.4	0.98
2,183	0.61	579.5	0.98
2,193	0.61	577.4	0.98
2,203	0.61	579.5	0.98
2,213	0.61	577.4	0.98
2,223	0.62	577.4	0.98
2,233	0.62	577.5	0.98
2,243	0.62	583.7	0.99
2,253	0.63	575.4	0.98
2,263	0.63	571.3	0.97
2,273	0.63	565.2	0.96
2,283	0.63	563.2	0.96
2,293	0.64	561.2	0.95
2,303	0.64	557.2	0.95
2,313	0.64	555.2	0.94
2,323	0.65	557.2	0.95
2,333	0.65	555.3	0.94
2,343	0.65	557.2	0.95
2,353	0.65	563.2	0.96
2,363	0.66	569.3	0.97
2,373	0.66	579.5	0.98
2,383	0.66	598.4	1.02
2,393	0.66	607	1.03
2,403	0.67	604.8	1.03
2,413	0.67	600.6	1.02
2,423	0.67	598.4	1.02
2,433	0.68	592	1.01
2,443	0.68	585.7	0.99
2,453	0.68	575.4	0.98
2,463	0.68	575.4	0.98

2,473	0.69	565.2	0.96
2,483	0.69	565.2	0.96
2,493	0.69	585.8	0.99
2,503	0.70	604.8	1.03
2,513	0.70	609.2	1.03
2,523	0.70	600.6	1.02
2,533	0.70	583.7	0.99
2,543	0.71	577.5	0.98
2,553	0.71	565.2	0.96
2,563	0.71	569.3	0.97
2,573	0.71	579.5	0.98
2,583	0.72	602.7	1.02
2,593	0.72	613.5	1.04
2,603	0.72	604.8	1.03
2,613	0.73	604.8	1.03
2,623	0.73	598.4	1.02
2,633	0.73	585.7	0.99
2,643	0.73	579.5	0.98
2,653	0.74	569.3	0.97
2,663	0.74	567.2	0.96
2,673	0.74	575.4	0.98
2,683	0.75	565.2	0.96
2,693	0.75	575.4	0.98
2,703	0.75	577.4	0.98
2,713	0.75	575.4	0.98
2,723	0.76	581.6	0.99
2,733	0.76	592	1.01
2,743	0.76	596.3	1.01
2,753	0.76	598.4	1.02
2,763	0.77	598.4	1.02
2,773	0.77	585.7	0.99
2,783	0.77	581.6	0.99
2,793	0.78	585.7	0.99
2,803	0.78	577.5	0.98
2,813	0.78	573.3	0.97
2,823	0.78	573.3	0.97
2,833	0.79	569.3	0.97
2,843	0.79	559.2	0.95
2,853	0.79	555.3	0.94
2,863	0.80	551.3	0.94
2,873	0.80	547.4	0.93
2,883	0.80	547.4	0.93
2,893	0.80	530.1	0.90
2,903	0.81	526.4	0.89
2,913	0.81	526.3	0.89
2,923	0.81	528.2	0.90
2,933	0.81	539.6	0.92
2,943	0.82	549.4	0.93
2,953	0.82	551.3	0.94
2,963	0.82	559.2	0.95

2,973	0.83	563.2	0.96
2,983	0.83	559.2	0.95
2,993	0.83	553.3	0.94
3,003	0.83	547.4	0.93
3,013	0.84	549.4	0.93
3,023	0.84	535.8	0.91
3,033	0.84	522.6	0.89
3,043	0.85	517.1	0.88
3,053	0.85	530.1	0.90
3,063	0.85	545.5	0.93
3,073	0.85	551.3	0.94
3,083	0.86	555.3	0.94
3,093	0.86	541.6	0.92
3,103	0.86	535.8	0.91
3,113	0.86	541.6	0.92
3,123	0.87	545.4	0.93
3,133	0.87	549.3	0.93
3,143	0.87	551.3	0.94
3,153	0.88	541.6	0.92
3,163	0.88	541.6	0.92
3,173	0.88	543.5	0.92
3,183	0.88	541.6	0.92
3,193	0.89	537.7	0.91
3,203	0.89	533.9	0.91
3,213	0.89	533.9	0.91
3,223	0.90	528.2	0.90
3,233	0.90	518.9	0.88
3,243	0.90	498.9	0.85
3,253	0.90	462.9	0.79
3,263	0.91	423.5	0.72
3,273	0.91	381.9	0.65
3,283	0.91	346.9	0.59
3,293	0.91	305.1	0.52
3,303	0.92	273.2	0.46
3,313	0.92	246.3	0.42
3,323	0.92	226.9	0.39
3,333	0.93	206.9	0.35
3,343	0.93	189.9	0.32
3,353	0.93	171.9	0.29
3,363	0.93	161.2	0.27
3,373	0.94	147.5	0.25
3,383	0.94	129.7	0.22
3,393	0.94	113.3	0.19
3,403	0.95	93.1	0.16
3,413	0.95	78.2	0.13
3,423	0.95	66.4	0.11
3,433	0.95	58.8	0.10
3,443	0.96	52.6	0.09
3,453	0.96	47.3	0.08
3,463	0.96	43.4	0.07

3,473	0.96	41.1	0.07
3,483	0.97	38.9	0.07
3,493	0.97	35.1	0.06
3,503	0.97	31	0.05
3,513	0.98	29.4	0.05
3,523	0.98	28.6	0.05
3,533	0.98	28.2	0.05
3,543	0.98	25.8	0.04
3,553	0.99	24.9	0.04
3,563	0.99	24.5	0.04
3,573	0.99	22.9	0.04
3,583	1.00	22.3	0.04
3,593	1.00	21.6	0.04
3,603	1.00	20.9	0.04
3,613	1.00	20.1	0.03
3,623	1.01	19.4	0.03
3,633	1.01	18.7	0.03
3,643	1.01	17.7	0.03
3,653	1.01	17.3	0.03
3,663	1.02	16.4	0.03
3,673	1.02	15.8	0.03
3,683	1.02	15.2	0.03
3,693	1.03	14.5	0.02
3,703	1.03	13.9	0.02
3,713	1.03	13.4	0.02
3,723	1.03	12.9	0.02
3,733	1.04	12.6	0.02
3,743	1.04	12.3	0.02
3,753	1.04	12.1	0.02
3,763	1.05	11.8	0.02
3,773	1.05	11.6	0.02
3,783	1.05	11.2	0.02
3,793	1.05	10.9	0.02
3,803	1.06	10.7	0.02
3,813	1.06	10.5	0.02
3,823	1.06	10.1	0.02
3,833	1.06	9.7	0.02
3,843	1.07	9.3	0.02
3,853	1.07	9.1	0.02
3,863	1.07	9	0.02
3,873	1.08	8.8	0.01
3,883	1.08	8.7	0.01
3,893	1.08	8.5	0.01
3,903	1.08	8.5	0.01
3,913	1.09	8.4	0.01
3,923	1.09	8.2	0.01
3,933	1.09	8.1	0.01
3,943	1.10	7.9	0.01
3,953	1.10	7.9	0.01
3,963	1.10	7.8	0.01

3,973	1.10	7.8	0.01
3,983	1.11	7.6	0.01
3,993	1.11	7.6	0.01
4,003	1.11	7.5	0.01
4,013	1.11	7.4	0.01
4,023	1.12	7.1	0.01
4,033	1.12	6.9	0.01
4,043	1.12	6.8	0.01
4,053	1.13	6.4	0.01
4,063	1.13	6.2	0.01
4,073	1.13	6.1	0.01
4,083	1.13	6	0.01
4,093	1.14	5.9	0.01
4,103	1.14	5.9	0.01
4,113	1.14	5.8	0.01
4,123	1.15	5.8	0.01
4,133	1.15	5.7	0.01
4,143	1.15	5.8	0.01
4,153	1.15	5.8	0.01
4,163	1.16	5.8	0.01
4,173	1.16	5.7	0.01
4,183	1.16	5.5	0.01
4,193	1.16	5.4	0.01
4,203	1.17	5.3	0.01
4,213	1.17	5.3	0.01
4,223	1.17	5.1	0.01
4,233	1.18	5.1	0.01
4,243	1.18	5.1	0.01
4,253	1.18	5.1	0.01
4,263	1.18	5.1	0.01
4,273	1.19	5.2	0.01
4,283	1.19	5.1	0.01
4,293	1.19	5.1	0.01
4,303	1.20	5.1	0.01
4,313	1.20	5	0.01
4,323	1.20	4.9	0.01
4,333	1.20	4.9	0.01
4,343	1.21	4.8	0.01
4,353	1.21	5	0.01
4,363	1.21	4.9	0.01
4,373	1.21	4.9	0.01
4,383	1.22	4.7	0.01
4,393	1.22	4.6	0.01
4,403	1.22	4.5	0.01
4,413	1.23	4.5	0.01
4,423	1.23	4.7	0.01
4,433	1.23	4.7	0.01
4,443	1.23	4.7	0.01
4,453	1.24	4.7	0.01
4,463	1.24	4.2	0.01

4,473	1.24	4.2	0.01
4,483	1.25	4.2	0.01
4,493	1.25	4.2	0.01
4,503	1.25	4.5	0.01
4,513	1.25	4.5	0.01
4,523	1.26	4.2	0.01
4,533	1.26	4.2	0.01
4,543	1.26	4.3	0.01
4,553	1.26	4.2	0.01
4,563	1.27	4.2	0.01
4,573	1.27	4.2	0.01
4,583	1.27	4.1	0.01
4,593	1.28	4	0.01
4,603	1.28	4	0.01
4,613	1.28	4	0.01
4,623	1.28	4	0.01
4,633	1.29	4	0.01
4,643	1.29	4	0.01
4,653	1.29	4	0.01
4,663	1.30	4	0.01
4,673	1.30	3.9	0.01
4,683	1.30	3.8	0.01
4,693	1.30	3.7	0.01
4,703	1.31	3.7	0.01
4,713	1.31	3.8	0.01
4,723	1.31	3.7	0.01
4,733	1.31	3.7	0.01
4,743	1.32	3.7	0.01
4,753	1.32	3.8	0.01
4,763	1.32	3.8	0.01
4,773	1.33	3.7	0.01
4,783	1.33	3.7	0.01
4,793	1.33	3.7	0.01
4,803	1.33	3.7	0.01
4,813	1.34	3.7	0.01
4,823	1.34	3.6	0.01
4,833	1.34	3.5	0.01
4,843	1.35	3.5	0.01
4,853	1.35	3.6	0.01
4,863	1.35	3.5	0.01
4,873	1.35	3.4	0.01
4,883	1.36	3.4	0.01
4,893	1.36	3.3	0.01
4,903	1.36	3.3	0.01
4,913	1.36	3.4	0.01
4,923	1.37	3.4	0.01
4,933	1.37	3.3	0.01
4,943	1.37	3.5	0.01
4,953	1.38	3.5	0.01
4,963	1.38	3.4	0.01

4,973	1.38	3.4	0.01
4,983	1.38	3.4	0.01
4,993	1.39	3.4	0.01
5,003	1.39	3.4	0.01
5,013	1.39	3.3	0.01
5,023	1.40	3.3	0.01
5,033	1.40	3.2	0.01
5,043	1.40	3.3	0.01
5,053	1.40	3.2	0.01
5,063	1.41	3.1	0.01
5,073	1.41	3.1	0.01
5,083	1.41	3.1	0.01
5,093	1.41	3.1	0.01
5,103	1.42	3.2	0.01
5,113	1.42	3.2	0.01
5,123	1.42	3.2	0.01
5,133	1.43	3.2	0.01
5,143	1.43	3.1	0.01
5,153	1.43	3.1	0.01
5,163	1.43	3	0.01
5,173	1.44	3	0.01
5,183	1.44	3.1	0.01
5,193	1.44	3.2	0.01
5,203	1.45	3.1	0.01
5,213	1.45	3	0.01
5,223	1.45	3	0.01
5,233	1.45	2.9	0.00
5,243	1.46	2.9	0.00
5,253	1.46	2.9	0.00
5,263	1.46	2.9	0.00
5,273	1.46	2.9	0.00
5,283	1.47	2.9	0.00
5,293	1.47	2.9	0.00
5,303	1.47	3	0.01
5,313	1.48	3	0.01
5,323	1.48	3.1	0.01
5,333	1.48	3.1	0.01
5,343	1.48	3.1	0.01
5,353	1.49	3.1	0.01
5,363	1.49	3.1	0.01
5,373	1.49	3.1	0.01
5,383	1.50	3	0.01
5,393	1.50	3	0.01
5,403	1.50	3	0.01
5,413	1.50	3	0.01
5,423	1.51	2.9	0.00
5,433	1.51	2.9	0.00
5,443	1.51	2.9	0.00
5,453	1.51	2.9	0.00
5,463	1.52	3	0.01

5,473	1.52	3.1	0.01
5,483	1.52	3.1	0.01
5,493	1.53	3	0.01
5,503	1.53	2.9	0.00
5,513	1.53	2.8	0.00
5,523	1.53	2.9	0.00
5,533	1.54	3	0.01
5,543	1.54	3	0.01
5,553	1.54	3	0.01
5,563	1.55	3	0.01
5,573	1.55	3	0.01
5,583	1.55	2.9	0.00
5,593	1.55	2.8	0.00
5,603	1.56	2.9	0.00
5,613	1.56	2.9	0.00
5,623	1.56	3	0.01
5,633	1.56	2.9	0.00
5,643	1.57	2.9	0.00
5,653	1.57	2.8	0.00
5,663	1.57	2.7	0.00
5,673	1.58	2.7	0.00
5,683	1.58	2.7	0.00
5,693	1.58	2.7	0.00
5,703	1.58	2.9	0.00
5,713	1.59	2.9	0.00
5,723	1.59	2.9	0.00
5,733	1.59	2.8	0.00
5,743	1.60	2.7	0.00
5,753	1.60	2.7	0.00
5,763	1.60	2.7	0.00
5,773	1.60	2.7	0.00
5,783	1.61	2.8	0.00
5,793	1.61	2.8	0.00
5,803	1.61	2.8	0.00
5,813	1.61	2.8	0.00
5,823	1.62	2.8	0.00
5,833	1.62	2.8	0.00
5,843	1.62	2.7	0.00
5,853	1.63	2.7	0.00
5,863	1.63	2.7	0.00
5,873	1.63	2.8	0.00
5,883	1.63	2.7	0.00
5,893	1.64	2.7	0.00
5,903	1.64	2.7	0.00
5,913	1.64	2.7	0.00
5,923	1.65	2.7	0.00
5,933	1.65	2.6	0.00
5,943	1.65	2.6	0.00
5,953	1.65	2.6	0.00
5,963	1.66	2.5	0.00

5,973	1.66	2.5	0.00
5,983	1.66	2.6	0.00
5,993	1.66	2.6	0.00
6,003	1.67	2.6	0.00
6,013	1.67	2.6	0.00
6,023	1.67	2.6	0.00
6,033	1.68	2.6	0.00
6,043	1.68	2.7	0.00
6,053	1.68	2.7	0.00
6,063	1.68	2.6	0.00
6,073	1.69	2.6	0.00
6,083	1.69	2.6	0.00
6,093	1.69	2.6	0.00
6,103	1.70	2.6	0.00
6,113	1.70	2.6	0.00
6,123	1.70	2.5	0.00
6,133	1.70	2.5	0.00
6,143	1.71	2.5	0.00
6,153	1.71	2.5	0.00
6,163	1.71	2.6	0.00
6,173	1.71	2.7	0.00
6,183	1.72	2.6	0.00
6,193	1.72	2.5	0.00
6,203	1.72	2.5	0.00
6,213	1.73	2.5	0.00
6,223	1.73	2.6	0.00
6,233	1.73	2.6	0.00
6,243	1.73	2.6	0.00
6,253	1.74	2.6	0.00
6,263	1.74	2.6	0.00
6,273	1.74	2.5	0.00
6,283	1.75	2.5	0.00
6,293	1.75	2.4	0.00
6,303	1.75	2.4	0.00
6,313	1.75	2.4	0.00
6,323	1.76	2.4	0.00
6,333	1.76	2.5	0.00
6,343	1.76	2.5	0.00
6,353	1.76	2.6	0.00
6,363	1.77	2.6	0.00
6,373	1.77	2.6	0.00
6,383	1.77	2.5	0.00
6,393	1.78	2.5	0.00
6,403	1.78	2.4	0.00
6,413	1.78	2.4	0.00
6,423	1.78	2.4	0.00
6,433	1.79	2.5	0.00
6,438.4	1.79	2.6	0.00
6,448.4	1.79	2.6	0.00
6,458.4	1.79	2.5	0.00

6,468.4	1.80	2.5	0.00
6,478.4	1.80	2.5	0.00
6,488.4	1.80	2.5	0.00
6,498.4	1.81	2.4	0.00
6,508.4	1.81	2.4	0.00
6,518.4	1.81	2.4	0.00
6,528.4	1.81	2.5	0.00
6,538.4	1.82	2.6	0.00
6,548.4	1.82	2.6	0.00
6,558.4	1.82	2.5	0.00
6,568.4	1.82	2.5	0.00
6,578.4	1.83	2.4	0.00
6,588.4	1.83	2.4	0.00
6,598.4	1.83	2.4	0.00
6,608.4	1.84	2.4	0.00
6,618.4	1.84	2.5	0.00